ESTIMATION OF THE LONGITUDINAL AND LATERAL VELOCITIES OF A VEHICLE USING EXTENDED KALMAN FILTERS

A Thesis
Presented to
The Academic Faculty

by

Juan Camilo Alvarez

In Partial Fulfillment
of the Requirements for the Degree
Master of Science in the
School of Electrical and Computer Engineering

Georgia Institute of Technology
December 2006

ESTIMATION OF THE LONGITUDINAL AND LATERAL VELOCITIES OF A VEHICLE USING EXTENDED KALMAN FILTERS

Approved by:

Professor David G. Taylor, Advisor
School of Electrical and Computer Engineering
Georgia Institute of Technology

Professor Magnus Egerstedt
School of Electrical and Computer Engineering
Georgia Institute of Technology

Professor Erik I. Verriest
School of Electrical and Computer Engineering
Georgia Institute of Technology

Date Approved: 15 November 2006

To my parents

ACKNOWLEDGEMENTS

It is with great pleasure that I'm saying thanks to all of you who have been encouraging and helping me during my academic years at Georgia Tech.

Firstly, I would like to thank my advisor, Dr David G. Taylor, with whom I spent many hours trying to find a solution to this tough problem. Thanks to his great experience, I finally developed my own approach.

I would also like to thank my parents and my brother, Alejandro, who have been an invaluable support for me across my entire life and especially now during the writing of my thesis.

Many thanks to the rest of my family and my friends in France, Spain, Colombia and the United States for all their help during these five years abroad from Colombia.

Finally, I gratefully acknowledge the Office of Graduate Affairs of the School of Electrical and Computer Engineering at the Georgia Institute of Technology for their help during this last year.

TABLE OF CONTENTS

LIST OF TABLES

LIST OF FIGURES

SUMMARY

Vehicle motion and tire forces have been estimated using extended Kalman filters for many years. The use of extended Kalman filters is primarily motivated by the simultaneous presence of nonlinear dynamics and sensor noise.

Two versions of extended Kalman filters are employed in this thesis: one using a deterministic tire-force model and the other using a stochastic tire-force model. Previous literature has focused on linear stochastic tire-force models and on linear deterministic tire-force models.

However, it is well known that there exists a nonlinear relationship between slip variables and tire-force variables. For this reason, it is suitable to use a nonlinear deterministic tire-force model for the extended Kalman filter, and this is the novel aspect of this work.

The objective of this research is to show the improvement of the extended Kalman filter using a nonlinear deterministic tire-force model in comparison to linear stochastic tire-force model. The simulation model is a seven degree-of-freedom bicycle model that includes vertical suspension dynamics but neglects the roll motion. A comparison between the linear stochastic tire-force model and the nonlinear deterministic tire-force model confirms the expected results. Simulation studies are performed on some illustrative examples obtaining good tracking performance.

CHAPTER I

INTRODUCTION

The need to reduce the risk of human lives and human errors while driving a vehicle in low-traction conditions, such as ice, snow, gravel or wet pavement, has motivated the development of electronic stability control systems. These systems have proven to be helpful in reducing vehicle crashes. Research in the area of systems and controls has improved these electronic stability control systems. The automotive industry has always had a goal of developing more accurate systems. Stability control systems use accelerometers, gyroscopes, and tachometers to measure certain signals. However, the components of the vehicle body velocity vector are needed to implement stability control systems, yet no sensor for these signals is available. For this reason, it is necessary to estimate the velocity vector of a vehicle accurately.

For the scientific community, velocity estimation is an old issue. In 1958, Wintergerst [30] tried to determine the velocity of moving bodies by means of the Doppler effect. Then, in 1966, Detchmendy [5] tried to solve the problem of controlling the attitude of a space vehicle using noisy measurements of one angular velocity. The motivation for this approach was to remove two of the three rate gyros from a space vehicle attitude-control system. However, all of these approaches were inaccurate due to the noise in the sensors.

During the 1960's, Rudolf E. Kalman developed an algorithm to solve the noise problem. The name of this algorithm is the Kalman filter. Thanks to this filter, the position and the velocity of an object can be estimated given only a sequence of observations, each of which includes some noise or error. In fact, the research in this field increased because of space industry. Many projects were trying to apply linear optimal control and filtering theories to space vehicles. In 1971, Mehra [11] tried to apply the Kalman filter theory to the velocity estimation problem. In [11], Mehra compared the performance of several non-linear filters for the real-time estimation of the trajectory of a re-entry vehicle from its radar

observations. Then, in 1979, Ramachandra [13] tried to solve the estimation problem using a one-dimensional dynamic model to estimate the optimum steady-state position, velocity and acceleration of a vehicle moving with a constant acceleration perturbed by a zero-mean plant noise. Ramachandra continued to work on this problem, and he published another paper, [14], in 1984. In this paper, Ramachandra used a two-dimensional Kalman tracking filter to obtain optimum estimates of position, velocity, and acceleration of an aircraft whose acceleration was perturbed due to maneuvers and/or other random factors.

However, velocity estimation in the space industry and in the automotive industry is approached differently due to tire-road friction. For this reason, in [8], Kiencke tried to estimate the adhesion characteristics during cornering by observing the lateral vehicle dynamics. In the following years, many researchers focused their efforts on this area of research. In Yi [31], Fukada [6], Stephant [21], Canudas [4], Muller [12], Lee [10], Wang [29], and Shim [18], the authors tried to estimate the tire-road friction coefficient by taking into account the nonlinear characteristics of tires. In [1], Alvarez also tried to estimate the tire-road friction coefficient using a LuGre dynamic model.

Other authors focused on other specific aspects of the vehicle. For example, Venhovens [28] worked in the application of stochastic state estimators in vehicle dynamic control. Moreover, Vahidi [27] estimated the vehicle mass and road grade, and Sivashankar [19] described a method for vehicle yaw rate estimation. Furthermore, during the three last years, Stephant focused on the estimation of vehicle sideslip angle in many articles [24], [23], [22], and [25]. Finally, in [26], Ungoren did a study in lateral speed estimation methods.

Since the global positioning system (GPS) was developed for the public market, some authors have worked in methods of estimating several vehicle states using GPS data. In [3], Bevly utilizes GPS velocity measurements to determine the inertial sensor errors using a kinematic Kalman filter estimator. In [7], Kehl describes a methodology to guide a vehicle along a predefined path using GPS measurements. In [17], Ryu estimates the sideslip angle, the longitudinal velocity, roll, and grade of a vehicle using inertial sensors and a GPS system.

However, in this thesis, the focus is on the comparison of the results of the paper "Nonlinear State and Tire Force Estimation for Advanced Vehicle Control," [15] that Laura

Ray published in 1995 with the results of a related approach proposed here for the first time. In this paper, Ray used a nine degree-of-freedom vehicle model and an analytic tire-force model to simulate true vehicle motion, and a five degree-of-freedom vehicle model to implement the Kalman filter. In [15], Ray tried to solve the velocity-estimation problem using a stochastic tire-force model. Ray used a set of sensors to measure the steer angle, the brake torque, the yaw rate, the front and rear wheel angular velocities, and the longitudinal and lateral accelerations of the vehicle. However, in [15], Ray did not consider the aspect of trying to use a nonlinear deterministic tire-force model, and, consequently, this is why Ray was obligated to measure brake torque (a signal that cannot realistically be measured). The proposed approach removes the need for brake torque measurement by replacing a linear stochastic tire-force model with a nonlinear deterministic tire-force model.

The purpose of this thesis is to implement extended Kalman filters to estimate the longitudinal and lateral velocities of a seven degree-of-freedom vehicle. Following is the approach used in this thesis:

First, the implementation of a kinematics-based estimation approach is discussed to show that this approach is not accurate. Then, the implementation of an extended Kalman filter is presented using a linear stochastic approach. The linear stochastic approach uses a stochastic tire-force model in the extended Kalman filter. After this, a nonlinear deterministic approach is implemented. For the nonlinear deterministic approach, a nonlinear deterministic tire-force model is used. Finally, a comparison between these two approaches is completed to show the improvement of the nonlinear deterministic approach over the linear stochastic approach.

CHAPTER II

VEHICLE MODEL

The purpose of this thesis is to implement extended Kalman filters to estimate the longitudinal and lateral velocities of a seven degree-of-freedom vehicle. However, before trying to do the implementation of the extended Kalman filters, it is critical to specify the real model that it is going to be used for the simulation of the vehicle.

2.1 Nonlinear Model

Computer simulations of the actual vehicle motion are going to be done using a high-order, nonlinear vehicle model and an analytic tire force model. The model used to do this simulation is the one described in [15]. The vehicle is only going to have a single front and rear wheel, no roll motion and the model includes vertical suspension dynamics. However, the model used in this thesis is different with respect to the model used in [15]. The simulation model is simpler than the model used in [15]. The vehicle is going to be on a flat road. Schematic and signs conventions corresponding to the seven degree-of-freedom vehicle are defined in Figure 1 and Figure 2.

2.1.1 Equations of Motion

Now, let's specify the equations of motion of the vehicle. The equations of motion are as follows:

$$\dot{v}_x = \frac{1}{m}\left[F_{xf}\cos\delta_f - F_{yf}\sin\delta_f + F_{xr}\right] + r\,v_y \tag{1}$$

$$\dot{v}_y = \frac{1}{m}\left[F_{yf}\cos\delta_f + F_{xf}\sin\delta_f + F_{yr}\right] - r\,v_y \tag{2}$$

$$\dot{r} = \frac{1}{I_z}\left[L_f(F_{xf}\sin\delta_f + F_{yf}\cos\delta_f) - L_r\,F_{yr}\right] \tag{3}$$

$$\dot{\omega}_f = \frac{1}{I_w}\left[-R_w F_{xf} - K_b T_b\right] \tag{4}$$

$$\dot{\omega}_r = \frac{1}{I_w}\left[-R_w F_{xr} - (1 - K_b) T_b\right] \tag{5}$$

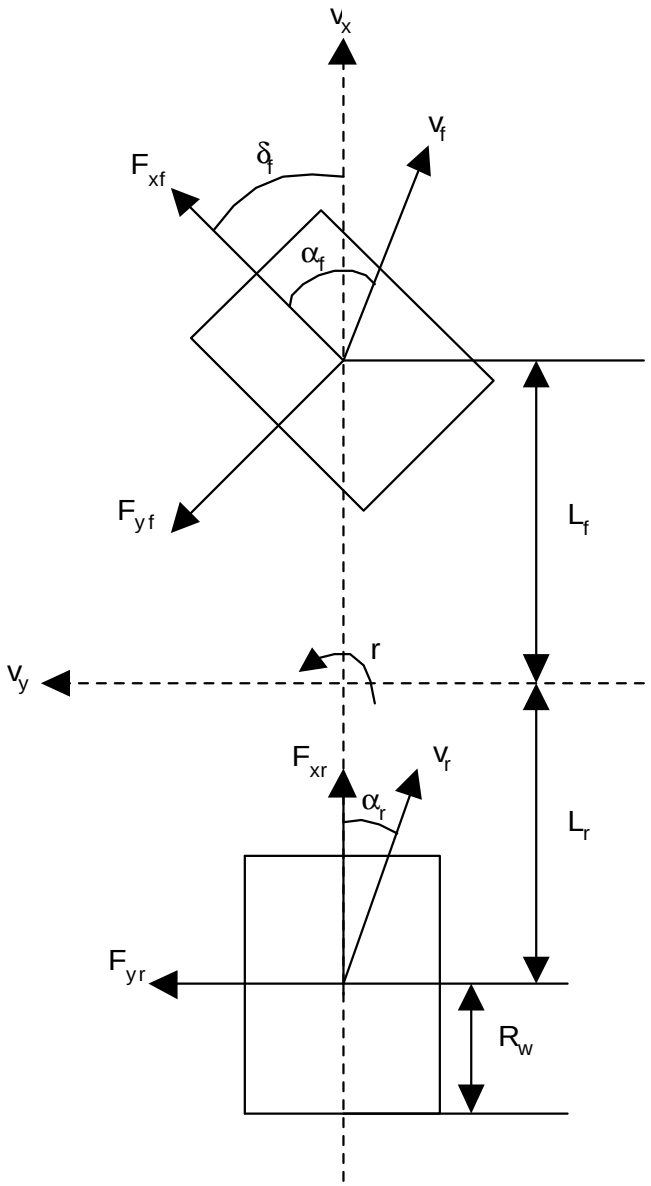

Figure 1: Seven degree-of-freedom bicycle model (top view).

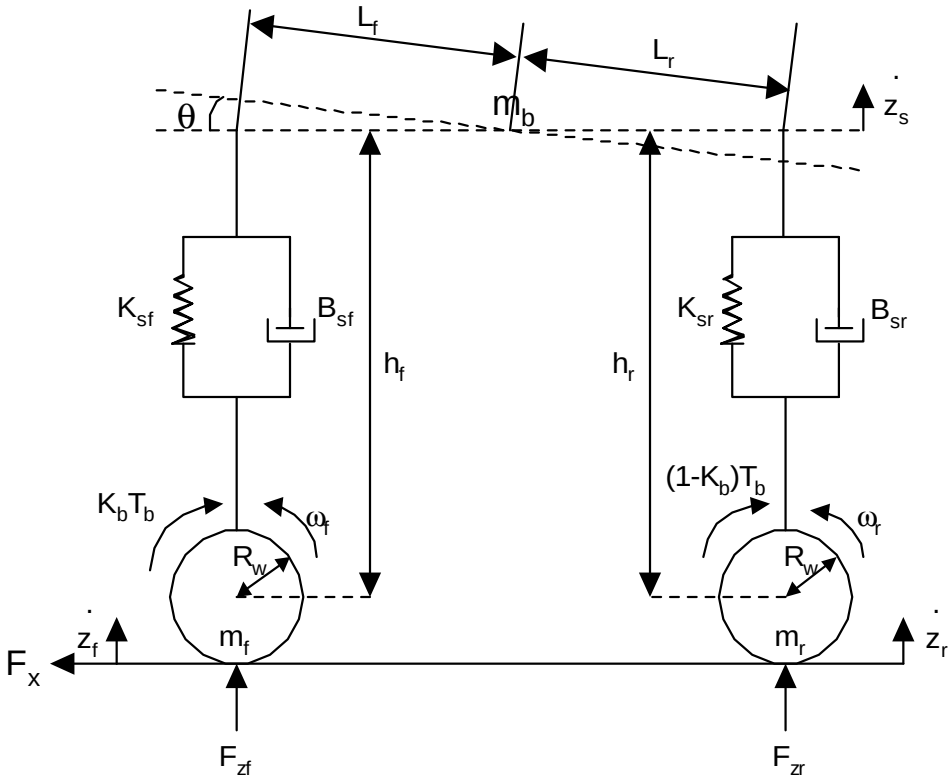

Figure 2: Seven degree-of-freedom bicycle model (side view).

where v_x and v_y are the longitudinal and lateral velocities respectively, r is the yaw rate, ω_f and ω_r are the front and rear wheel angular velocities, δ_f is the front steer angle, T_b is the applied braking torque, and F_{xf}, F_{yf}, F_{xr} and F_{yr} are the front and rear longitudinal and lateral tire forces. For small θ, using Figures 1 and 2, the following equations can be written:

$$\ddot{z}_s = \frac{1}{m_b}[-K_{sf}(z_s + L_f\theta) - B_{sf}(\dot{z}_s + L_f\dot{\theta}) - K_{sr}(z_s - L_r\theta) - B_{sr}(\dot{z}_s - L_r\dot{\theta})] \quad (6)$$

$$\begin{aligned}\ddot{\theta} = \frac{1}{I_p}\{&-(h_f + R_w)F_{xf}\cos\delta_f + (h_f + R_w)F_{yf}\sin\delta_f - (h_r + R_w)F_{xr} \\ &- L_f[K_{sf}(z_s + L_f\theta) + B_{sf}(\dot{z}_s + L_f\dot{\theta})] \\ &+ L_r[K_{sr}(z_s - L_r\theta) + B_{sr}(\dot{z}_s - L_r\dot{\theta})]\}\end{aligned} \quad (7)$$

where z_s is the sprung mass vertical displacement, θ is the body pitch angle, $\dot{z}_s$ is the first time derivative of the sprung mass vertical displacement, and $\dot{\theta}$ is the first time derivative of the body pitch angle. For this model, the following state vector is going to be used:

$$x(t) = [v_x\, v_y\, r\, \omega_f\, \omega_r\, z_s\, \theta\, \dot{z}_s\, \dot{\theta}]^T \quad (8)$$

In the model, m is the total mass, m_b is the mass of the vehicle without the mass of the front and rear wheels m_f and m_r, R_w is the radius of the wheel, L_f is the distance from the center of gravity to the front axle, L_r is the distance from the center of gravity to the rear axle, h_f is the vertical distance from the center of gravity to the center of the front wheel at equilibrium, h_r is the vertical distance from the center of gravity to the center of the rear wheel at equilibrium, I_z is the moment of inertia of the vehicle about its yaw axis, I_w is the moment of inertia of the wheel about its axle, I_p is the moment of inertia of the vehicle about its roll axis, K_b is the fixed proportion of braking applied to the front wheel. The spring and damping constants K_{sf}, B_{sf}, K_{sr} and B_{sr} in (6) and (7) are the lumped parameters associated with the passive suspension system and tires.

2.1.2 Inputs and Outputs

The input vector of the real model is as follows:

$$u_1(t) = [\delta_f\, T_b] \quad (9)$$

The measurement equation (or output equation) is as follows:

$$z(t) = [r\,\omega_f\,\omega_r\,a_x\,a_y]^T + n(t) \tag{10}$$

where a_x and a_y are the longitudinal and lateral accelerations of the vehicle. $n(t)$ is a white Gaussian measurement noise. The variance of n is R. a_x and a_y can be written as:

$$a_x = \dot{v}_x - r\,v_y \tag{11}$$

$$a_y = \dot{v}_y + r\,v_x \tag{12}$$

The control inputs and the outputs are measured using a set of sensors. All these sensors are assumed to be on the vehicle. To measure the signals, accelerometers, gyroscopes, tachometers, torque sensors, and position sensors are used.

2.2 Tire Model

In this section, the tire model is going to be described. The tire model is used to simulate the true tire forces of the vehicle. The tire model that is going to be used is the one in [9]. The front and rear normal forces at the tire-road interface are as follows:

$$F_{zf} = -K_{sf}(z_s + L_f\theta) - B_{sf}(\dot{z}_s + L_f\dot{\theta}) + m_f g + m_b\frac{L_r}{L_f + L_r}g \tag{13}$$

$$F_{zr} = -K_{sr}(z_s - L_r\theta) - B_{sr}(\dot{z}_s - L_r\dot{\theta}) + m_r g + m_b\frac{L_f}{L_f + L_r}g \tag{14}$$

where g is the acceleration of gravity. The front and rear wheel slip angles α_f and α_r are as follows:

$$\alpha_f = \delta_f - \tan^{-1}\left(\frac{v_y + L_f\,r}{v_x}\right) \tag{15}$$

$$\alpha_r = -\tan^{-1}\left(\frac{v_y - L_r\,r}{v_x}\right) \tag{16}$$

The magnitudes of the front and rear axle velocities are as follows:

$$v_f = \sqrt{(v_y + L_f\,r)^2 + v_x^2} \tag{17}$$

$$v_r = \sqrt{(v_y - L_r\,r)^2 + v_x^2} \tag{18}$$

The front and rear longitudinal and lateral wheel slips are as follows:

$$\begin{bmatrix} s_{xf} \\ s_{yf} \end{bmatrix} = \frac{1}{v_f}\begin{bmatrix} R_w\,\omega_f\cos\alpha_f - v_f \\ R_w\,\omega_f\sin\alpha_f \end{bmatrix} \tag{19}$$

$$\begin{bmatrix} s_{xr} \\ s_{yr} \end{bmatrix} = \frac{1}{v_r} \begin{bmatrix} R_w\,\omega_r \cos\alpha_r \;-\; v_r \\ R_w\,\omega_r \sin\alpha_r \end{bmatrix} \tag{20}$$

The resultant front and rear wheel slips are as follows:

$$s_{res_f} \;=\; \sqrt{s_{xf}^2 \;+\; s_{yf}^2} \tag{21}$$

$$s_{res_r} \;=\; \sqrt{s_{xr}^2 \;+\; s_{yr}^2} \tag{22}$$

However, it is essential to know the friction coefficient μ to have a tire model. Therefore, the resultant front and rear friction coefficients are as follows:

$$\mu_{res_f} \;=\; (c_1(1 \;-\; e^{-c_2\,s_{res_f}}) \;-\; c_3\,s_{res_f})\lambda \tag{23}$$

$$\mu_{res_r} \;=\; (c_1(1 \;-\; e^{-c_2\,s_{res_r}}) \;-\; c_3\,s_{res_r})\lambda \tag{24}$$

where c_1, c_2, and c_3 are the Burckhardt coefficients, and λ is a scalar. Now, the front and rear longitudinal and lateral tire forces can be known accurately. The tire-force equations are as follows:

$$\begin{bmatrix} F_{xf} \\ F_{yf} \end{bmatrix} = \frac{\mu_{res_f}}{s_{res_f}} F_{zf} \begin{bmatrix} s_{xf} \\ s_{yf} \end{bmatrix} \tag{25}$$

$$\begin{bmatrix} F_{xr} \\ F_{yr} \end{bmatrix} = \frac{\mu_{res_r}}{s_{res_r}} F_{zr} \begin{bmatrix} s_{xr} \\ s_{yr} \end{bmatrix} \tag{26}$$

Consequently, the true model of the vehicle is as follows:

$$\dot{x}(t) \;=\; f[x(t)\,,\,u_1(t)] \tag{27}$$

$$z(t) \;=\; h[x(t)\,,\,u_1(t)] \;+\; n(t) \tag{28}$$

where $f[x(t)\,,\,u_1(t)]$ and $h[x(t)\,,\,u_1(t)]$ are specified using equations (1) to (7) and equations (10) to (26) respectively.

2.3 Simulation

In this section, we are going to simulate the true model. Firstly, we are going to specify the simulation parameters, the Burckhardt coefficients, the inputs and the initial conditions for the state vector of the true model.

The software Matlab is used for the simulation. It is well known that the theory is different from the practice when an algorithm is written in a computer. Therefore, some problems to implement a simulation in a computer have been found. In theory, the equations that we presented in this chapter are the right ones for the model of the vehicle. However, in the tire model we have equations (25) and (26), and if the slip is zero, the numerator and the denominator are both zero and the computer cannot calculate the forces. For this reason, an `if else` has been integrated into the algorithm.

L'Hopital's Rule has been used to solve this problem. Thanks to equations (13) to (26), F_{xf} and F_{yf} can be written as:

$$\begin{bmatrix} F_{xf} \\ F_{yf} \end{bmatrix} = \begin{bmatrix} \frac{(c_1(1-e^{-c_2\, s_{res_f}}) - c_3\, s_{res_f})\lambda\, F_{zf}\, s_{xf}}{s_{res_f}} \\ \frac{(c_1(1-e^{-c_2\, s_{res_f}}) - c_3\, s_{res_f})\lambda\, F_{zf}\, s_{yf}}{s_{res_f}} \end{bmatrix} \tag{29}$$

From equation (21), s_{xf} and s_{yf} are the x and y components of the vector where s_{res_f} is the magnitude. In the first equation of equation (29), s_{xf} is not a problem because if the resultant of the vector goes to zero, the components x and y of the vector also goes to zero. Moreover, F_{zf} is not dependent on s_{res_f} due to equation (13), and λ is a scalar. Therefore, the focus is only on $\frac{(c_1(1-e^{-c_2\, s_{res_f}}) - c_3\, s_{res_f})}{s_{res_f}}$.

To use l'Hopital's Rule, the derivation of the numerator and the denominator of this fraction with respect to s_{res_f} must be done. Therefore, the result is as follows:

$$\lim_{s_{res_f} \to 0} c_1\, c_2\, e^{-c_2\, s_{res_f}} \; - \; c_3 = c_1\, c_2 \; - \; c_3 \tag{30}$$

Consequently, the end result is as follows:

$$\lim_{s_{res_f} \to 0} F_{xf} = 0 \tag{31}$$

Therefore, the following assumption is made to simulate the system in the computer:

$$\begin{aligned} &\texttt{if} \qquad s_{res_f} > 0.001 \\ &\qquad\quad F_{xf} = \tfrac{\mu_{res_f}}{s_{res_f}} F_{zf} s_{xf} \\ &\texttt{else} \\ &\qquad\quad F_{xf} = 0 \end{aligned} \tag{32}$$

Table 1: Simulation Parameters

Parameter	**Value**	**Parameter**	**Value**
m	1301 kg	R_w	0.33 m
m_b	1171 kg	I_w	4.07 kg-m^2
m_f	70 kg	K_{sf}	30000 N/m
m_r	60 kg	K_{sr}	35000 N/m
L_f	1 m	B_{sf}	5000 N-s/m
L_r	1.45 m	B_{sr}	4500 N-s/m
I_z	1627 kg-m^2	I_p	2035 kg-m^2
h_f	0.53 m	K_b	0.6
h_r	0.52 m	g	9.81 m/s^2

Table 2: Burckhardt Coefficients

Parameter	**Value**
c_1	1
c_2	26
c_3	0.25

The case for F_{yf} is treated in the same way.

The simulation parameters and the Burckhardt coefficients are given in Tables 1 and 2. The real plant is doing the following: the inputs $T_b = 1400$ N-m and $\delta_f = 0.05$ rad are applied at $t = 0$, and at $t = 1.8$ sec these inputs change to $T_b = 0$ N-m and $\delta_f = 0$ rad. Moreover, at $t = 0.6$ sec, the coefficient of friction μ changes from 0.85 to 0.3. The Burckhardt coefficients in Table 2 gives a coefficient of friction μ of 0.85. Consequently, for $t \leq 0.6$, $\lambda = 1$, and for $t > 0.6$, $\lambda = \frac{0.3}{0.85}$. The simulation stops at $t = 3$ sec. For the true model, the inputs δ_f and T_b are shown in Figure 3.

In the following equations, v_{x_0}, ω_{f_0}, and ω_{r_0} are the initial conditions for the longitudinal velocity, and the front and rear wheel angular velocities. The values taken for v_{x_0}, ω_{f_0}, and ω_{r_0} in the simulation are as follows:

$$v_{x_0} = 25\,\text{m/s} \tag{33}$$

$$\omega_{f_0} = \frac{v_{x_0}}{R_w}\,\text{rad/s} \tag{34}$$

$$\omega_{r_0} = \frac{v_{x_0}}{R_w}\,\text{rad/s} \tag{35}$$

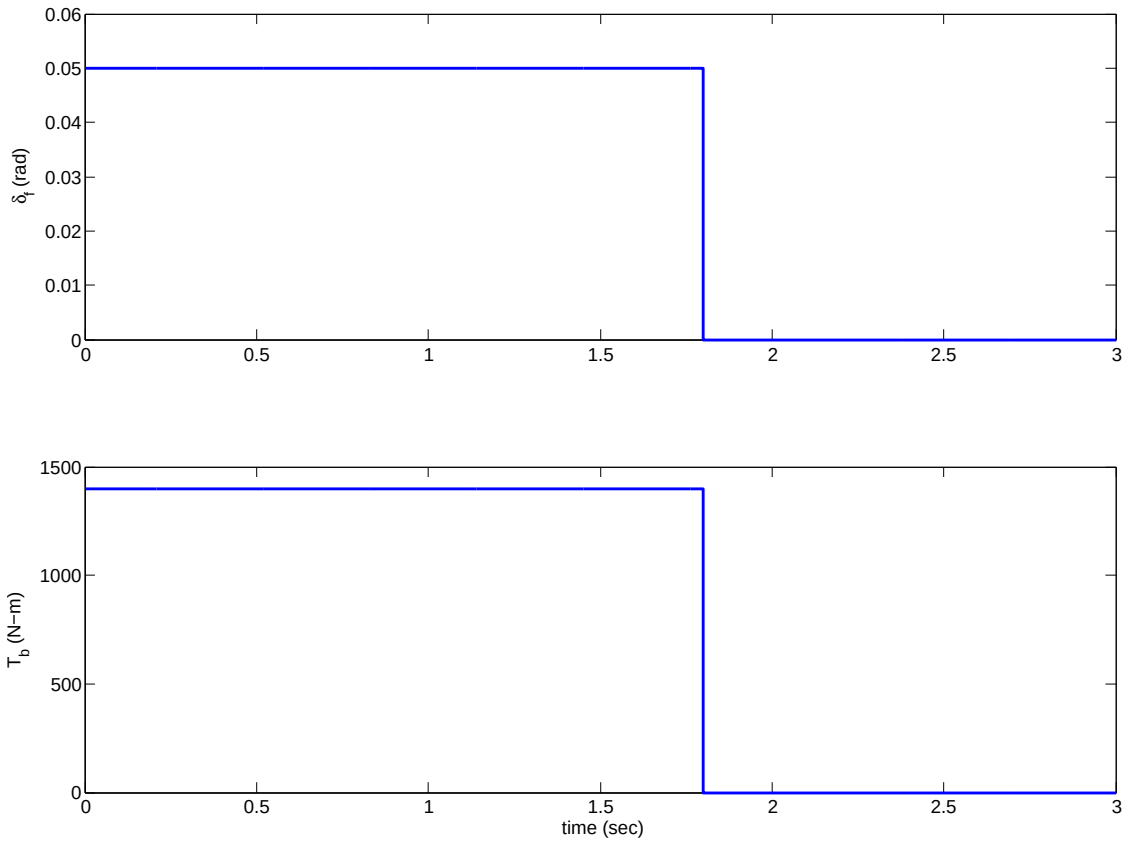

Figure 3: Inputs δ_f and T_b for the true model.

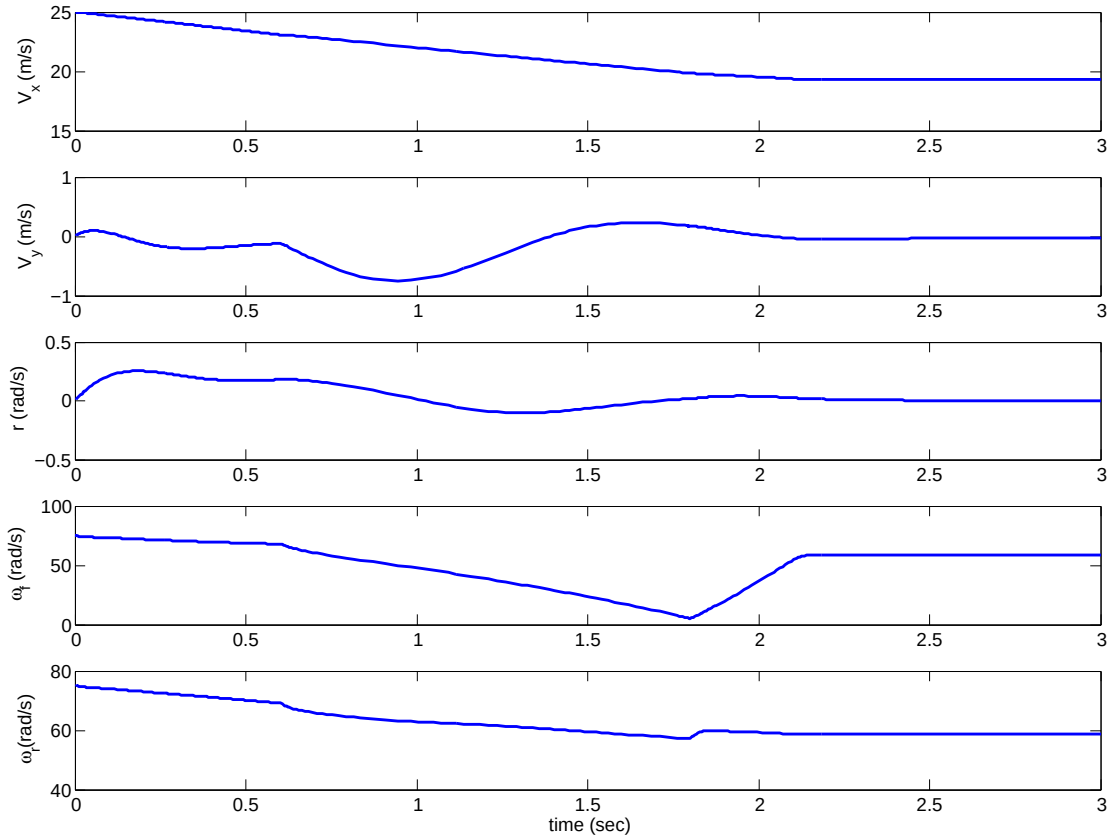

Figure 4: States v_x, v_y, r, ω_f, and ω_r for the true model.

For the true model, the initial state vector (8) is as follows:

$$x_0 = [v_{x_0},\, 0,\, 0,\, \omega_{f_0},\, \omega_{r_0},\, 0,\, 0,\, 0,\, 0]^T \tag{36}$$

The states v_x, v_y, r, ω_f, and ω_r are shown in Figure 4.

In Figure 5, a trajectory of the vehicle on the plane is represented. At time $t < 0$, the vehicle is in straight ahead driving. Then, at time $t \geq 0$, the vehicle starts to brake and to turn until $t = 1.8$ sec, while the coefficient of friction μ is changing at time $t = 0.6$ sec.

2.4 Kinematics-Based Estimation

In this section, we are going to see if the true motion of the vehicle can be estimated using a kinematics approach. The vehicle is considered as a rigid body, and here the wheels of

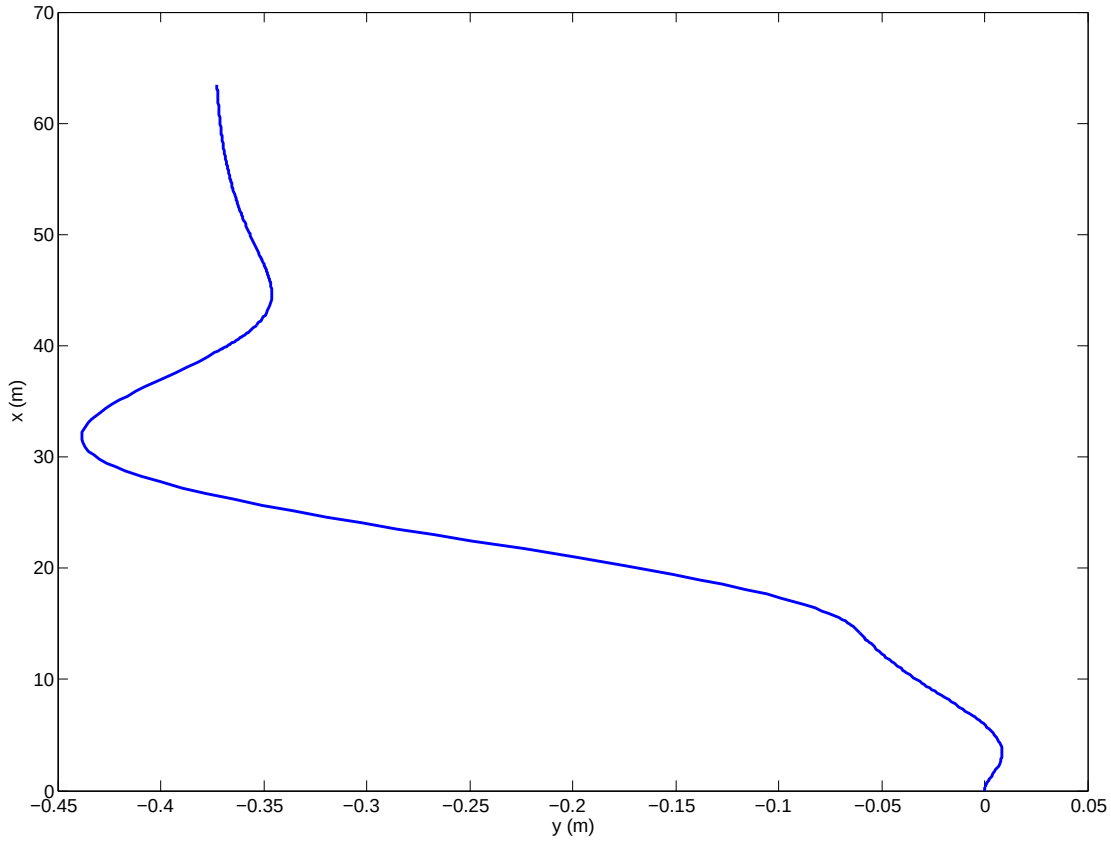

Figure 5: Trajectory of the vehicle on the plane.

the vehicle are not taken into account. Equations (17) and (18) can be written as:

$$\vec{v}_f = \begin{bmatrix} v_x \\ v_y \, + \, L_f \, r \end{bmatrix} \tag{37}$$

$$\vec{v}_r = \begin{bmatrix} v_x \\ v_y \, - \, L_r \, r \end{bmatrix} \tag{38}$$

In this section, we assume zero slip. For this reason, vectors ω_f and v_f agree in magnitude and in direction. Therefore, we have

$$\vec{v}_f = \begin{bmatrix} R_w \, \omega_f \cos \delta_f \\ R_w \, \omega_f \sin \delta_f \end{bmatrix} \tag{39}$$

Using the same idea for ω_r and v_r, we have

$$\vec{v}_r = \begin{bmatrix} R_w \, \omega_r \\ 0 \end{bmatrix} \tag{40}$$

Thanks to equations (37), (38), (39), and (40), we find the following equations for v_x and v_y:

$$\begin{bmatrix} v_x \\ v_y \end{bmatrix} = \begin{bmatrix} R_w \, \omega_f \cos \delta_f \\ R_w \, \omega_f \sin \delta_f \, - \, L_f \, r \end{bmatrix} \tag{41}$$

$$\begin{bmatrix} v_x \\ v_y \end{bmatrix} = \begin{bmatrix} R_w \, \omega_r \\ L_r \, r \end{bmatrix} \tag{42}$$

Due to (41) and (42), we have two ways to calculate v_x and v_y. For this reason, we are going to do the average between these two methods to calculate v_x and v_y. Finally, for the kinematics approach, v_x and v_y can be written as:

$$\begin{bmatrix} v_x \\ v_y \end{bmatrix} = \begin{bmatrix} \frac{R_w \, \omega_f \cos \delta_f + R_w \, \omega_r}{2} \\ \frac{R_w \, \omega_f \sin \delta_f - L_f \, r + L_r \, r}{2} \end{bmatrix} \tag{43}$$

From Figure 6, we can see that the kinematics approach is not accurate. We can conclude that we have a tradeoff, if we want to rely on simple equations, the estimator is going to be really simple, but with easy computations, we have a lot of error. We see that

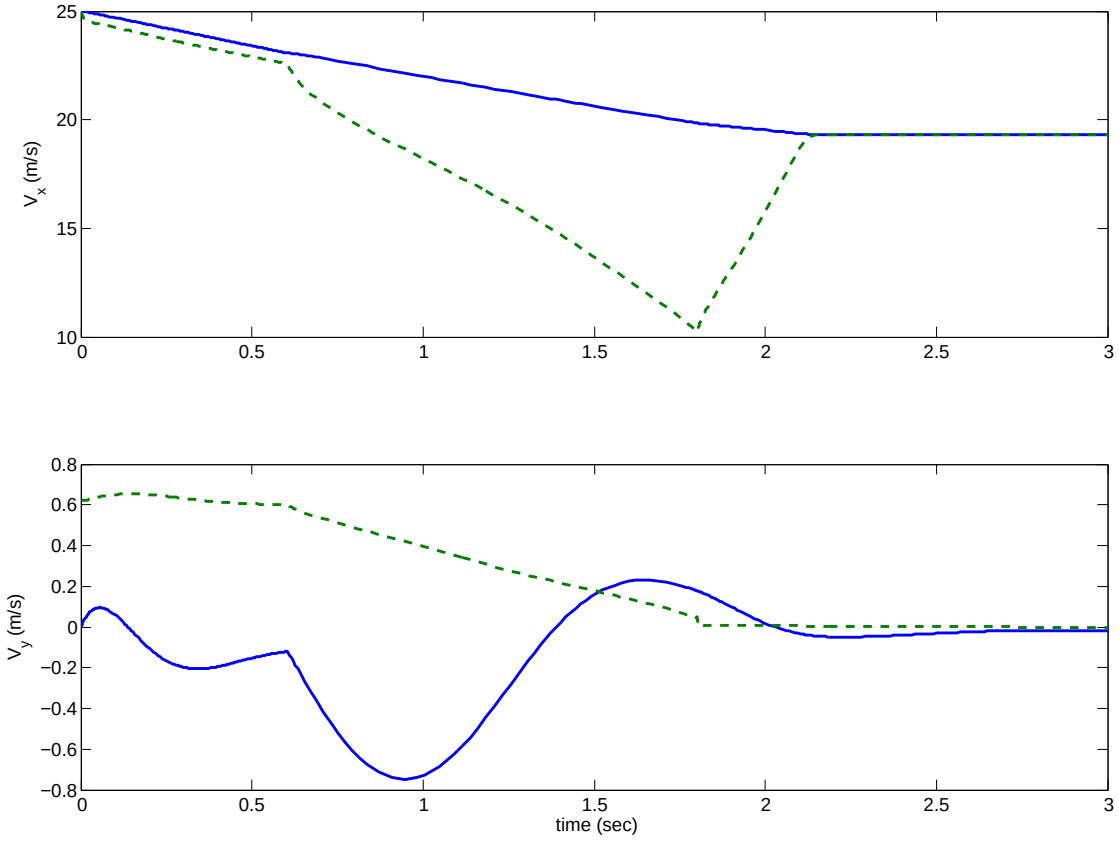

Figure 6: Actual Motion (solid lines) and State Estimates (dashed lines) for v_x and v_y for the Kinematics Approach.

we cannot assume zero slip. Slipping wheels can only be considered with friction model and dynamics. For this reason, let's consider now the linear stochastic approach and the nonlinear deterministic approach using an extended Kalman filter.

CHAPTER III

EXTENDED KALMAN FILTERS

3.1 Linear Stochastic Approach

3.1.1 Design Model

In the linear stochastic approach, the design model is different from the simulation model. For the design model, not all the equations specified in the previous chapter are used, only equations (1) to (5). In this approach, the suspension dynamics are neglected but the state vector $x(t)$ is augmented using differential equations for each force. To model each force, the model in [20] is used. The model is the following:

$$\begin{bmatrix} \dot{f}_0 \\ \dot{f}_1 \\ \dot{f}_2 \end{bmatrix} = \begin{bmatrix} 0 & 1 & 0 \\ 0 & 0 & 1 \\ 0 & 0 & 0 \end{bmatrix} \begin{bmatrix} f_0 \\ f_1 \\ f_2 \end{bmatrix} + w \tag{44}$$

where f_0 is the force, f_1 and f_2 are first and second derivatives of the force, and w is a white Gaussian noise. The variance of w is Q. This model is used for F_{xf}, F_{yf}, F_{xr} and F_{yr}. Now, the state vector for this design model is as follows:

$$x_{des}(t) = [v_x\, v_y\, r\, \omega_f\, \omega_r\, F_{xf}\, \dot{F}_{xf}\, \ddot{F}_{xf}\, F_{yf}\, \dot{F}_{yf}\, \ddot{F}_{yf}\, F_{xr}\, \dot{F}_{xr}\, \ddot{F}_{xr}\, F_{yr}\, \dot{F}_{yr}\, \ddot{F}_{yr}]^T \tag{45}$$

The input vector is the same as in equation (9).

3.1.2 Implementation of the Extended Kalman Filter

In this section, an extended Kalman filter is described for the purpose of estimating the state vector and the tire forces F_{xf}, F_{yf}, F_{xr} and F_{yr} of the design model. For the extended Kalman filter, the state vector is as follows:

$$\hat{x}_{des}(t) = [\hat{v}_x\, \hat{v}_y\, \hat{r}\, \hat{\omega}_f\, \hat{\omega}_r\, \hat{F}_{xf}\, \dot{\hat{F}}_{xf}\, \ddot{\hat{F}}_{xf}\, \hat{F}_{yf}\, \dot{\hat{F}}_{yf}\, \ddot{\hat{F}}_{yf}\, \hat{F}_{xr}\, \dot{\hat{F}}_{xr}\, \ddot{\hat{F}}_{xr}\, \hat{F}_{yr}\, \dot{\hat{F}}_{yr}\, \ddot{\hat{F}}_{yr}]^T \tag{46}$$

The continuous extended Kalman filter is implemented using Matlab and the `ode45` function. The filter equations are as follows:

$$\dot{\hat{x}}_{des}(t) \;=\; \tilde{f}_1(\hat{x}_{des}(t), u_1(t)) \,+\, K(t)[z(t) - h(\hat{x}_{des}(t), u_1(t))] \tag{47}$$

$$K(t) = P(t)B^T(t)R^{-1}(t) \tag{48}$$

$$\dot{P}(t) = A(t)P(t) + P(t)A^T(t) + L(t)Q(t)L^T(t) - K(t)R(t)K^{-1}(t) \tag{49}$$

where

$$A(t) = \left.\frac{\partial \tilde{f}_1}{\partial x_{des}}\right|_{\hat{x}_{des}} \tag{50}$$

$$L(t) = \frac{\partial \tilde{f}_1}{\partial w} \tag{51}$$

$$B(t) = \left.\frac{\partial h}{\partial x_{des}}\right|_{\hat{x}_{des}} \tag{52}$$

$$Q(t) = E(w(t)w(t)^T) \tag{53}$$

$$R(t) = E(n(t)n(t)^T) \tag{54}$$

$\tilde{f}_1$ is defined using equations (1) to (5), and (44) for each force F_{xf}, F_{yf}, F_{xr} and F_{yr}.

3.2 Nonlinear Deterministic Approach

3.2.1 Design Model

In the nonlinear deterministic approach, for the design model, equations (1) to (3), and (6) to (7) from the simulation model are used. Moreover, we are also going to estimate the scalar λ in (23) and (24) using the following equation:

$$\dot{\lambda} = 0 \tag{55}$$

Therefore, the state vector for the design model is as follows:

$$x_{des}(t) = [v_x\, v_y\, r\, z_s\, \dot{z}_s\, \theta\, \dot{\theta}\, \lambda]^T \tag{56}$$

In contrast to the linear stochastic approach which uses the friction model in (44), for the nonlinear deterministic approach, the suspension states z_s, $\dot{z}_s$, θ, and $\dot{\theta}$ are in the state vector for the design model (56). We need these suspension states to know the normal forces F_{zf} and F_{zr} in (13) and (14) to calculate the friction model. Moreover, the input vector is different from the simulation model. The input vector is as follows:

$$u_2(t) = [\delta_f\, \omega_f\, \omega_r] \tag{57}$$

Note that brake torque is not included as in (9).

3.2.2 Implementation of the Extended Kalman Filter

An extended Kalman filter is used to estimate the state vector and the tire forces F_{xf}, F_{yf}, F_{xr} and F_{yr} of the design model. For the extended Kalman filter, the state vector is as follows:

$$\hat{x}_{des}(t) = [\hat{v}_x\, \hat{v}_y\, \hat{r}\, \hat{z}_s\, \dot{\hat{z}}_s\, \hat{\theta}\, \dot{\hat{\theta}}\, \hat{\lambda}]^T \tag{58}$$

The continuous extended Kalman filter for this approach is also implemented using Matlab and the `ode45` function. The filter equations are as follows:

$$\dot{\hat{x}}_{des}(t) = \tilde{f}_2(\hat{x}_{des}(t), u_2(t)) + K(t)[z(t) - h(\hat{x}_{des}(t), u_2(t))] \tag{59}$$

$$K(t) = P(t)B^T(t)R^{-1}(t) \tag{60}$$

$$\dot{P}(t) = A(t)P(t) + P(t)A^T(t) - K(t)R(t)K^{-1}(t) \tag{61}$$

where

$$A(t) = \left.\frac{\partial \tilde{f}_2}{\partial x_{des}}\right|_{\hat{x}_{des}} \tag{62}$$

$$L(t) = \frac{\partial \tilde{f}_2}{\partial w} \tag{63}$$

$$B(t) = \left.\frac{\partial h}{\partial x_{des}}\right|_{\hat{x}_{des}} \tag{64}$$

$$R(t) = E(n(t)n(t)^T) \tag{65}$$

$\tilde{f}_2$ is defined using equations (1) to (3), (6) to (7), and (55).

CHAPTER IV

SIMULATION AND RESULTS

In this Chapter, a comparison between the linear stochastic approach and the nonlinear deterministic approach is done. The simulation parameters and the Burckhardt coefficients are given in Tables 1 and 2 in Chapter 2. The equation (32) is also used to implement the extended Kalman filter in both approaches. The real plant is going to behave as in Chapter 2. For the linear stochastic approach, the initial conditions are as follows:

$$\hat{x}_{des_0} = [v_{x_0} - e,\, e,\, e,\, \omega_{f_0},\, \omega_{r_0},\, 0,\, 0,\, 0,\, 0,\, 0,\, 0,\, 0,\, 0,\, 0,\, 0,\, 0,\, 0]^T \tag{66}$$

where (66) is the initial extended Kalman filter state vector (see equation (46)), and e represents an offset between the true value and the assumed value in the filter. The error covariance matrix for the extended Kalman filter P_0 is initialized with a 17×17 diagonal matrix with 10^6 in the diagonal. $R(t)$ and $Q(t)$ are the variances of the noises $n(t)$ and $w(t)$ of the equations (10) and (44). We have

$$E(n(t)n(s)^T) = R_0\delta_{ts} \tag{67}$$

$$E(w(t)w(s)^T) = Q_0\delta_{ts} \tag{68}$$

where R_0 is a 5×5 diagonal matrix with the vector [0.00001, 0.1, 0.1, 0.01, 0.01] in the diagonal, and Q_0 is a 17×17 diagonal matrix with 0.1 in the diagonal. For the nonlinear deterministic approach, the initial conditions are as follows:

$$\hat{x}_{des_0} = [v_{x_0} - e,\, e,\, e,\, 0,\, 0,\, 0,\, 0,\, 1.1]^T \tag{69}$$

where (69) is the initial extended Kalman filter state vector (see equation (58)). For the simulation, in the extended Kalman filter, λ is initialized with an error of 0.1 (see equations (23) and (24)). The error covariance matrix for the extended Kalman filter P_0 is initialized with an 8×8 diagonal matrix with 10^6 in the diagonal. $R(t)$ is the variance of the noise

$n(t)$ of the equation (10). We have

$$E(n(t)n(s)^T) = R_0\delta_{ts} \tag{70}$$

where R_0 is a 5×5 diagonal matrix with the vector [0.00001, 0.1, 0.1, 0.01, 0.01] in the diagonal.

Eight different simulations are done using 4 different values for e for each approach. The values used for e are 0.1, 0.3, 0.5, and 1. For the case $e = 0.1$, for v_x, the linear stochastic approach tracks the true signal a little bit better than the nonlinear deterministic approach (see Figures 7 and 8). However, for v_y, r, and the forces F_{xf}, F_{yf}, F_{xr} and F_{yr}, the nonlinear deterministic approach has better results than the linear stochastic approach (see Figures 7 to 10). For the case $e = 0.3$, for v_x, v_y, r, and the forces F_{xf}, F_{yf}, F_{xr} and F_{yr}, the nonlinear deterministic approach has better results in comparison to the linear stochastic approach (see Figures 11 to 14). For the case $e = 0.5$, for v_x, v_y, r, and the forces F_{xf}, F_{yf}, F_{xr} and F_{yr}, the nonlinear deterministic approach has better results than the linear stochastic approach (see Figures 15 to 18). For the case $e = 1$, for v_x, v_y, r, and the forces F_{xf}, F_{yf}, F_{xr} and F_{yr}, the results of the nonlinear deterministic approach are better than the results of the linear stochastic approach (see Figures 19 to 22).

However, these simulations are done in Matlab using the `ode45` function with an error tolerance of 0.0008. In fact, we have a tradeoff between the precision of the results and the number of points that we calculate for the simulation. For Matlab, an "estimated error in each integration step must satisfy `|e(i)|<=max(RelTol*abs(y(i)),AbsTol(i)`" where `y` is the solution vector. This error must be less than or equal to the acceptable error, which is a function of the specified relative tolerance, `RelTol`, and the specified absolute tolerance, `AbsTol`. Matlab defines the relative error tolerance as "a measure of the error relative to the size of each solution component." The relative error tolerance applies to all components of the solution vector. In fact, it controls the number of correct digits in all solution components, except those smaller than thresholds `AbsTol(i)`. For Matlab, `AbsTol(i)` is "a threshold below which the value of the $\texttt{i}^{\texttt{th}}$ solution component is unimportant." Absolute error tolerances apply to the individual components of the solution vector. The absolute

Table 3: Time Step Statistics

	Linear Stochastic Approach	**Nonlinear Deterministic Approach**
Minimum	5.02×10^{-13}	1.91×10^{-18}
Average	6.66×10^{-5}	3.20×10^{-5}

error tolerances determine the accuracy when the solution approaches zero.

In Figures 7 to 22, the data have been produced using `ode45` with `RelTol` and `AbsTol` both equal to 0.0008. This was done in an effort to make the comparison between the two extended Kalman filters fair. However, close inspection of Figures 7 to 22 reveals that the plant signals computed for the two cases are somewhat different. This undesirable feature must be related to the lengths of the time steps selected by `ode45`. In fact, the time step statistics are as shown in Table 3. Since the nonlinear deterministic case is computed with smaller steps, it is believed that the plant signals exhibited for that case are more accurate.

To summarize, for all the cases $e = 0.1$, $e = 0.3$, $e = 0.5$, and $e = 1$, the nonlinear deterministic approach tracks better the true signal than the linear stochastic approach in this kind of comparison (see Figures 7 to 22).

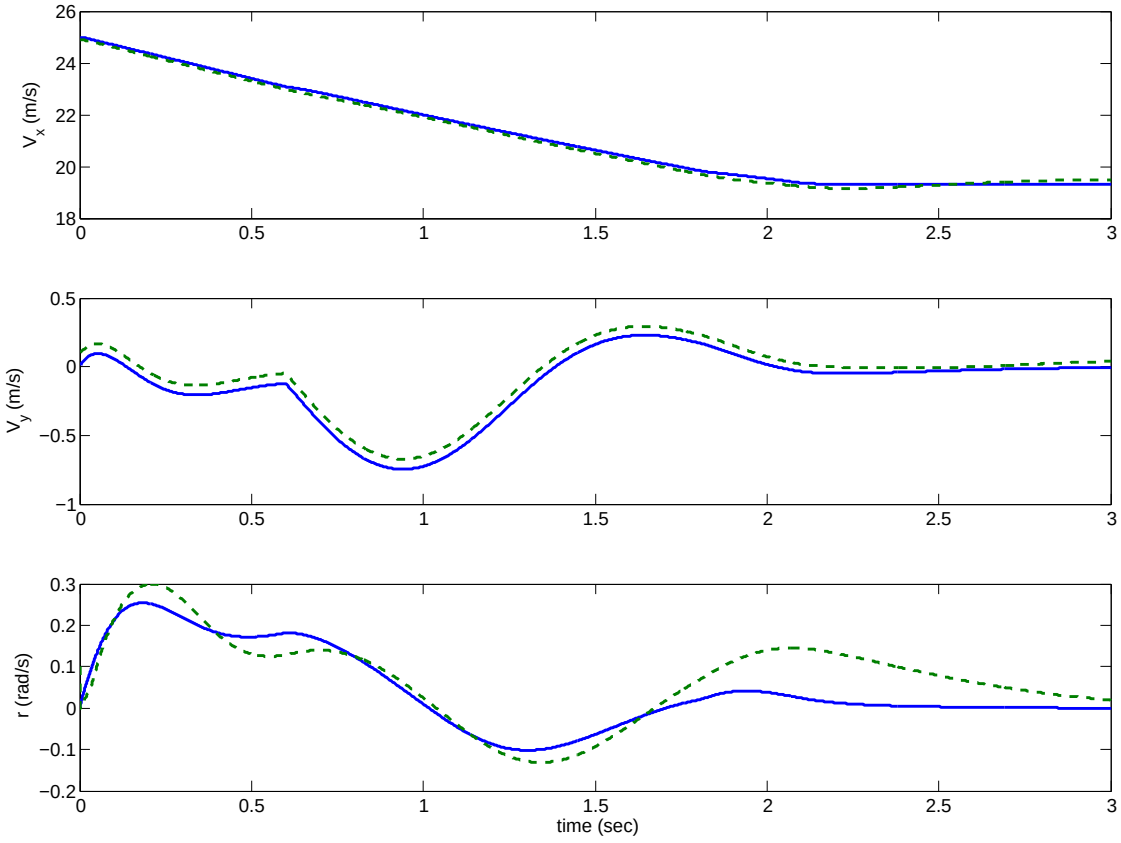

Figure 7: Actual Motion (solid lines) and State Estimates (dashed lines) for v_x, v_y, and r for the Linear Stochastic Approach with $e = 0.1$.

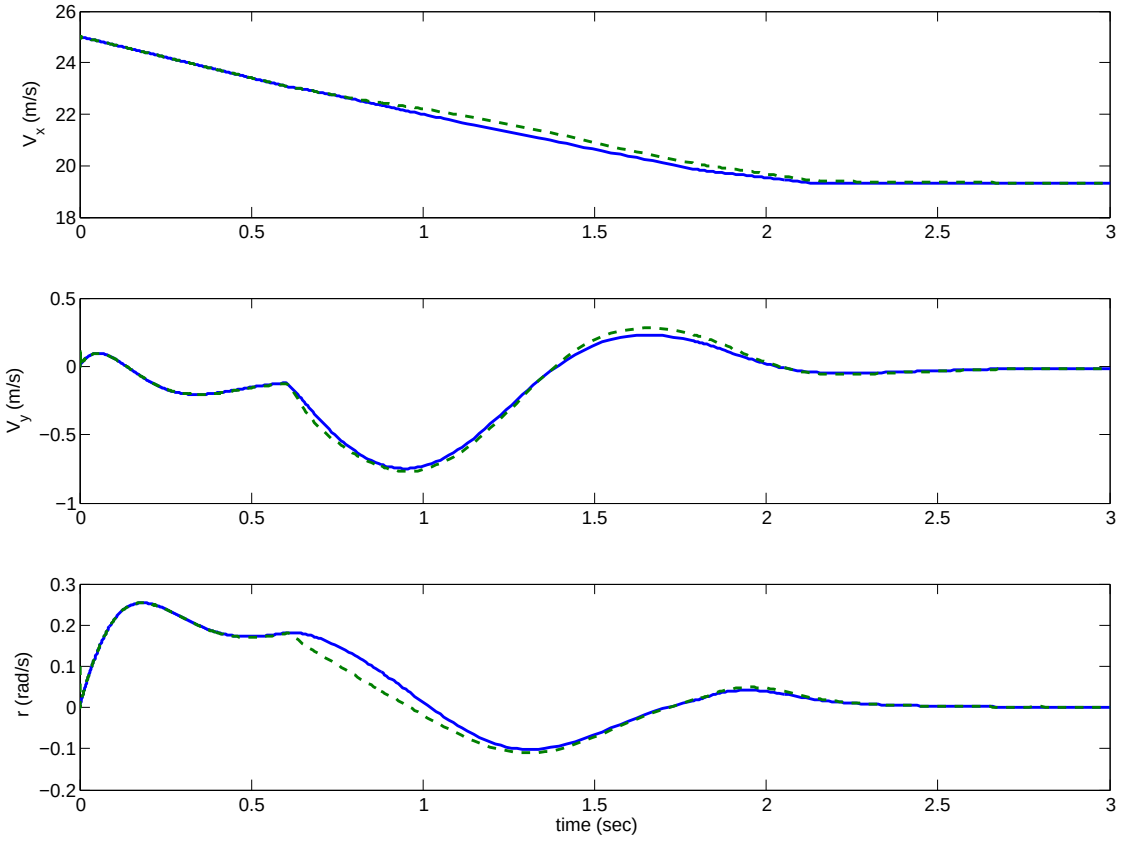

Figure 8: Actual Motion (solid lines) and State Estimates (dashed lines) for v_x, v_y, and r for the Nonlinear Deterministic Approach with $e = 0.1$.

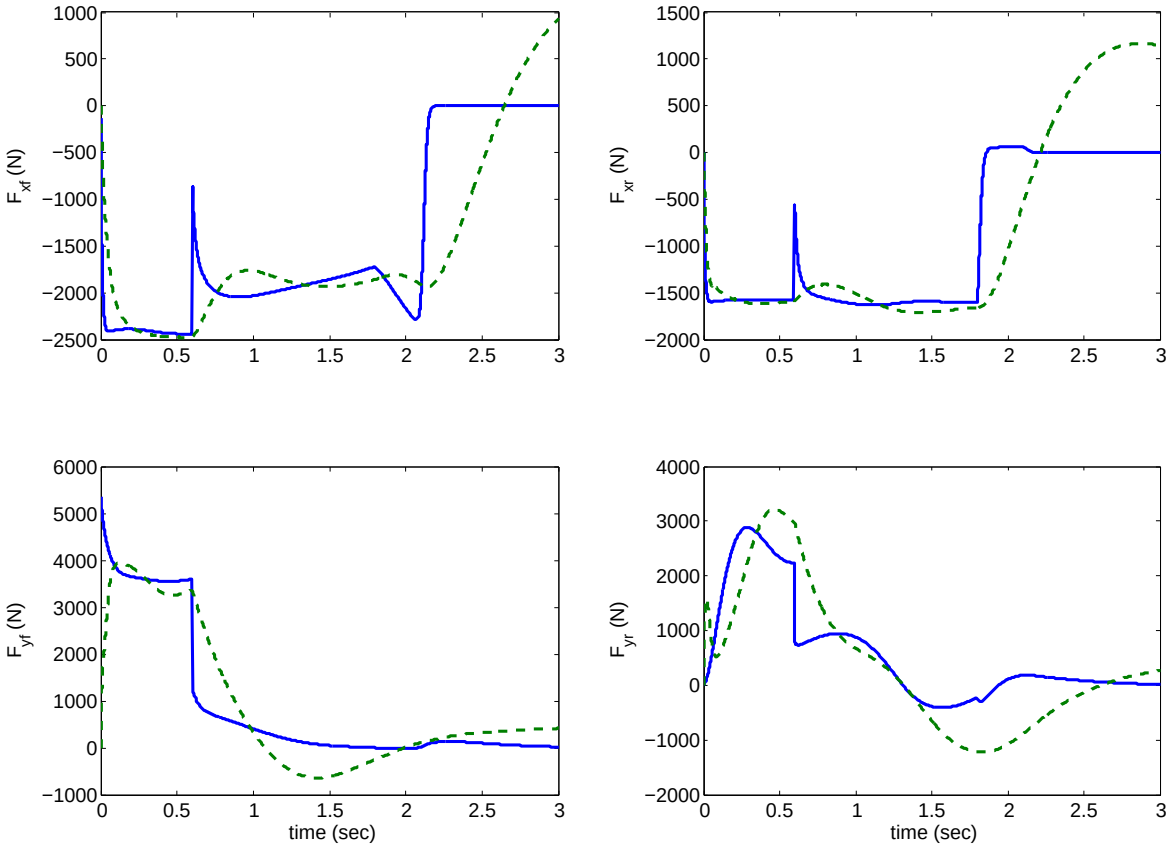

Figure 9: Actual Motion (solid lines) and State Estimates (dashed lines) for F_{xf}, F_{yf}, F_{xr} and F_{yr} for the Linear Stochastic Approach with $e = 0.1$.

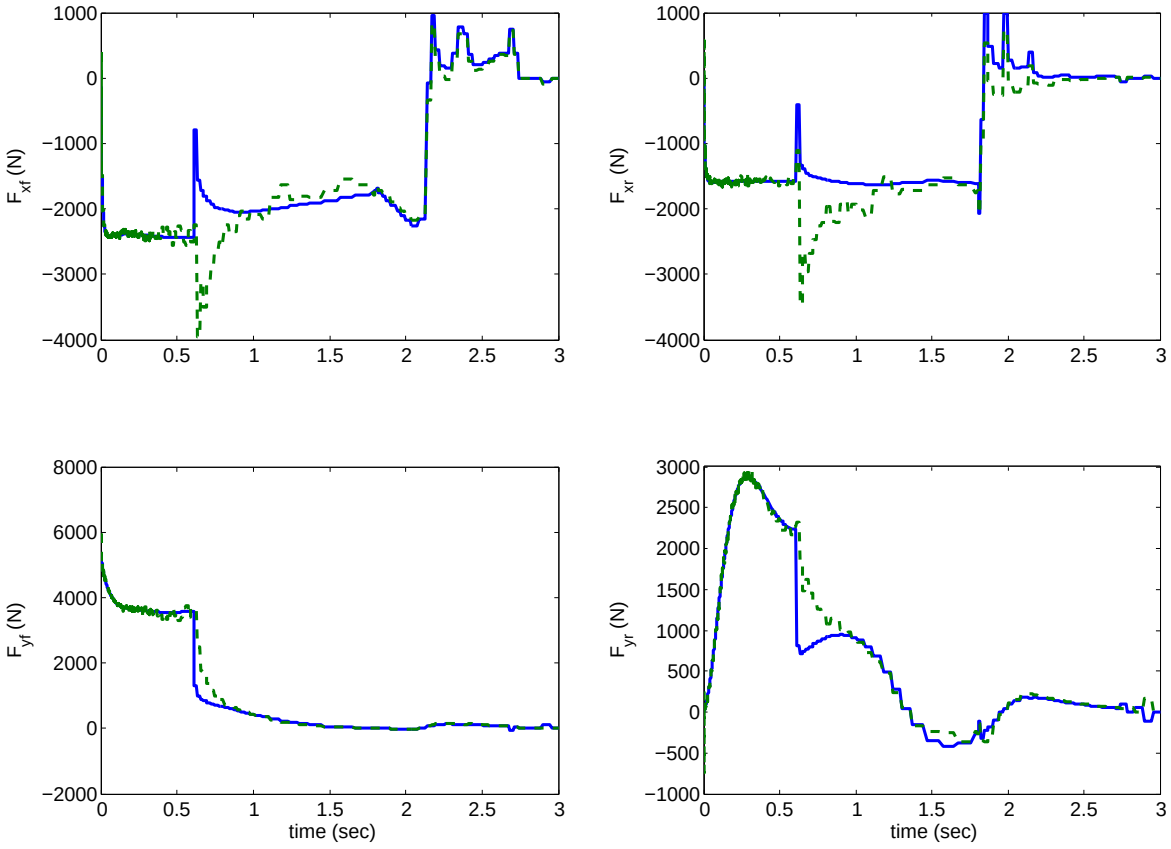

Figure 10: Actual Motion (solid lines) and State Estimates (dashed lines) for F_{xf}, F_{yf}, F_{xr} and F_{yr} for the Nonlinear Deterministic Approach with $e = 0.1$.

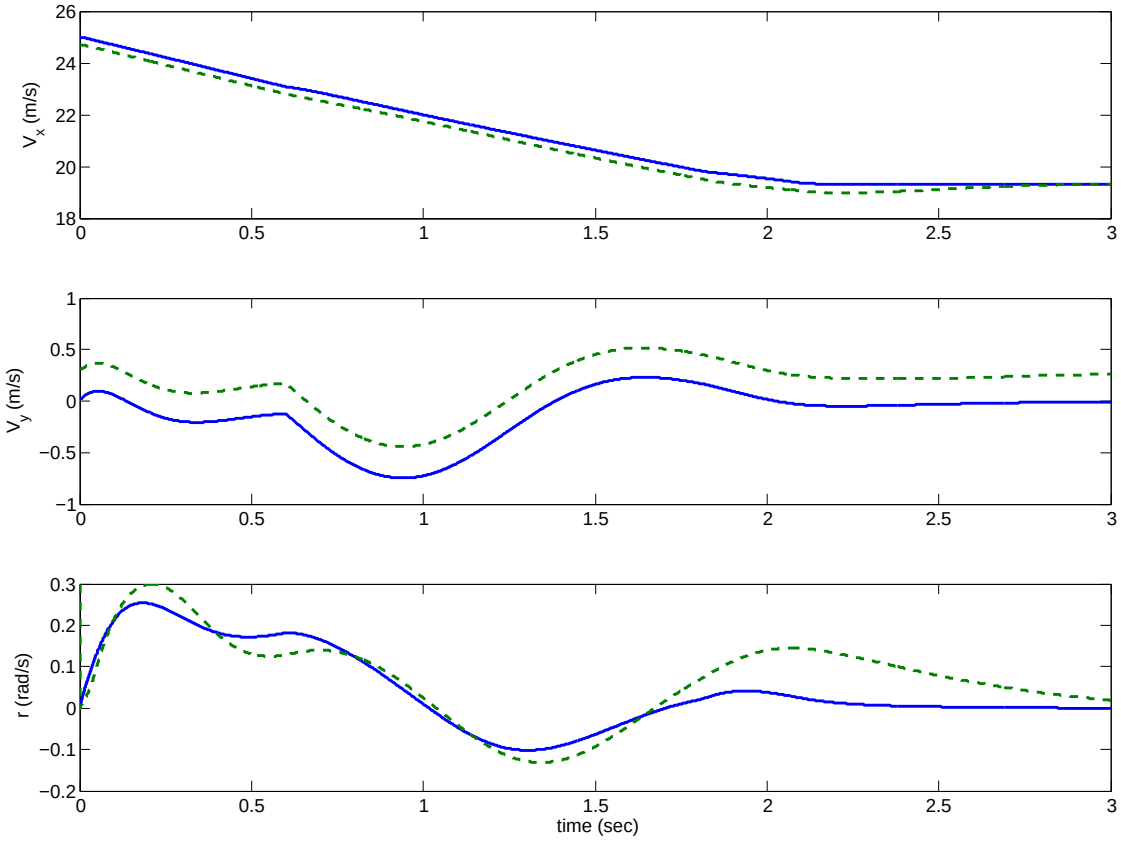

Figure 11: Actual Motion (solid lines) and State Estimates (dashed lines) for v_x, v_y, and r for the Linear Stochastic Approach with $e = 0.3$.

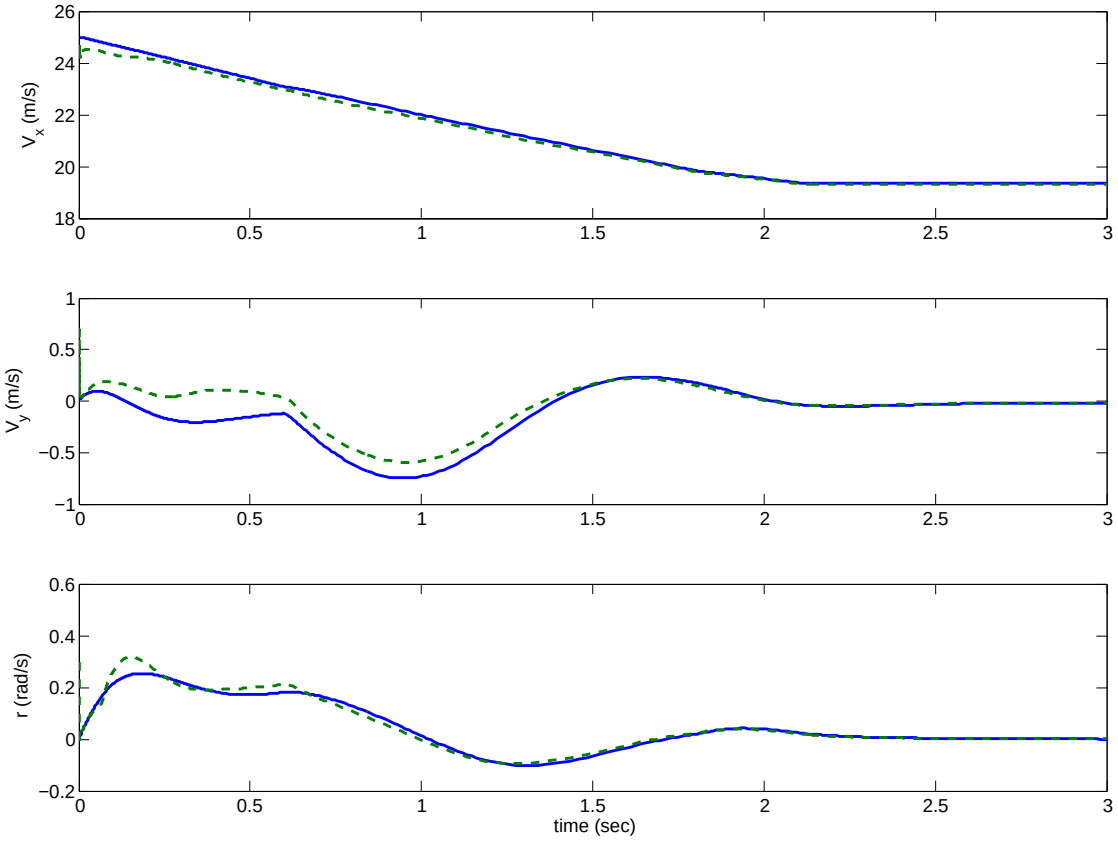

Figure 12: Actual Motion (solid lines) and State Estimates (dashed lines) for v_x, v_y, and r for the Nonlinear Deterministic Approach with $e = 0.3$.

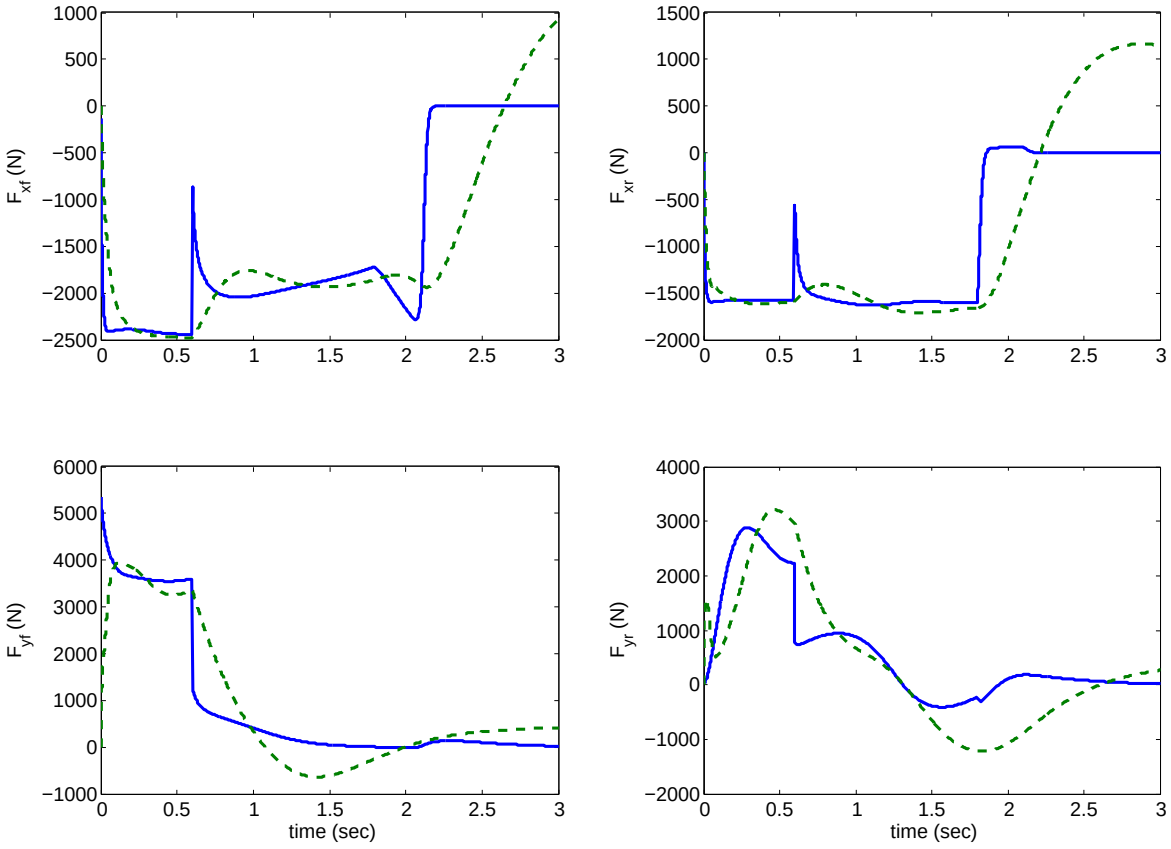

Figure 13: Actual Motion (solid lines) and State Estimates (dashed lines) for F_{xf}, F_{yf}, F_{xr} and F_{yr} for the Linear Stochastic Approach with $e = 0.3$.

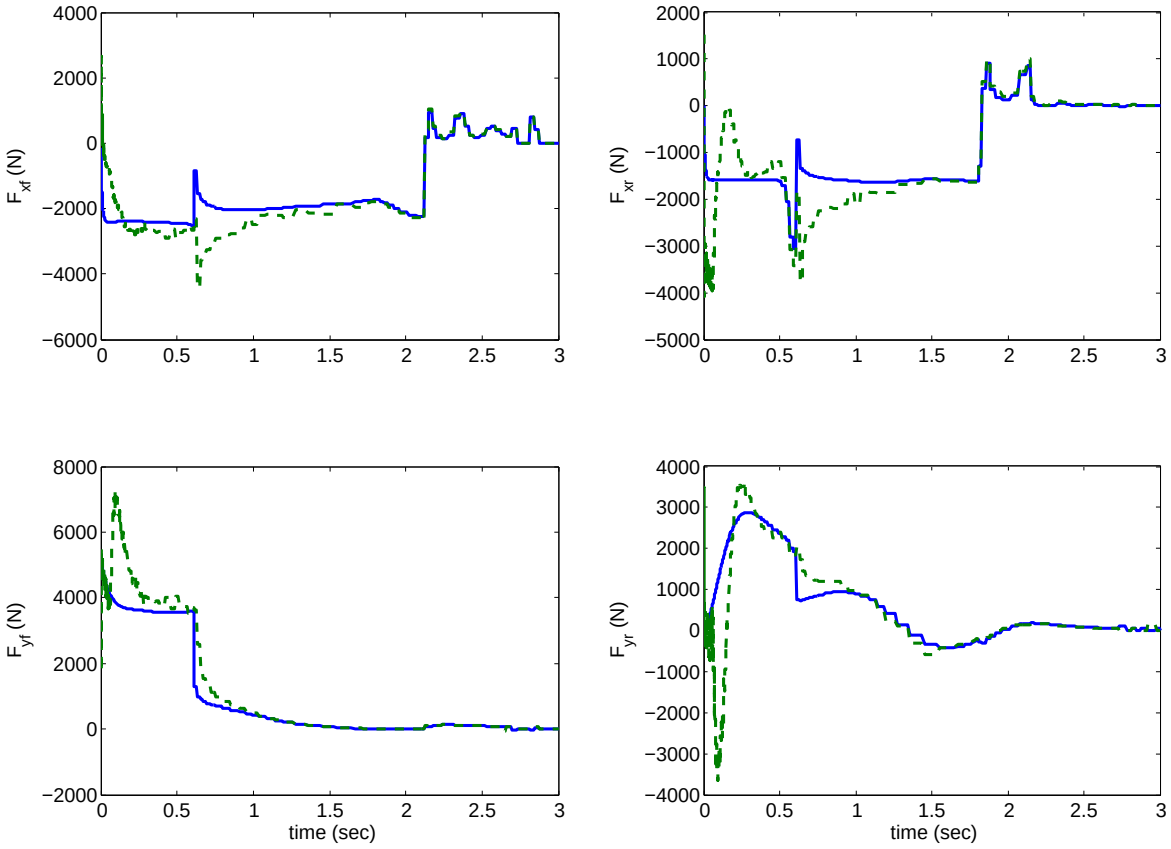

Figure 14: Actual Motion (solid lines) and State Estimates (dashed lines) for F_{xf}, F_{yf}, F_{xr} and F_{yr} for the Nonlinear Deterministic Approach with $e = 0.3$.

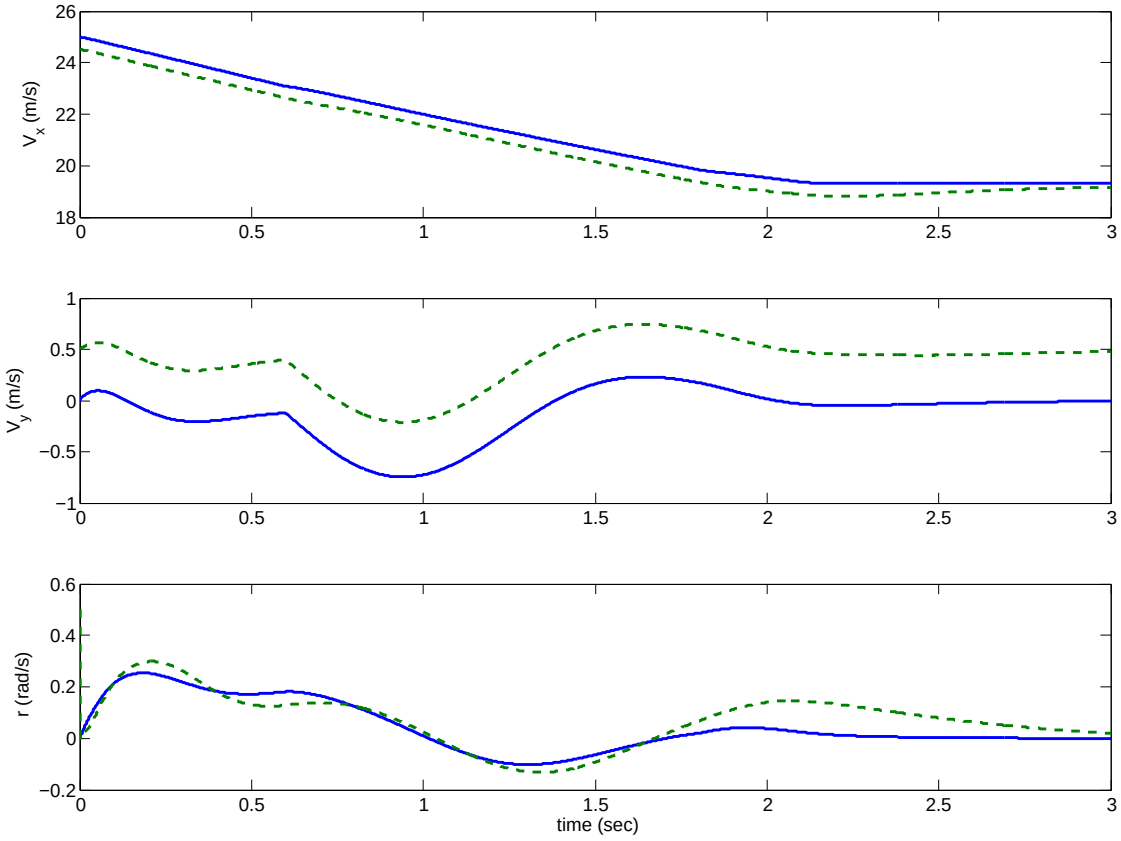

Figure 15: Actual Motion (solid lines) and State Estimates (dashed lines) for v_x, v_y, and r for the Linear Stochastic Approach with $e = 0.5$.

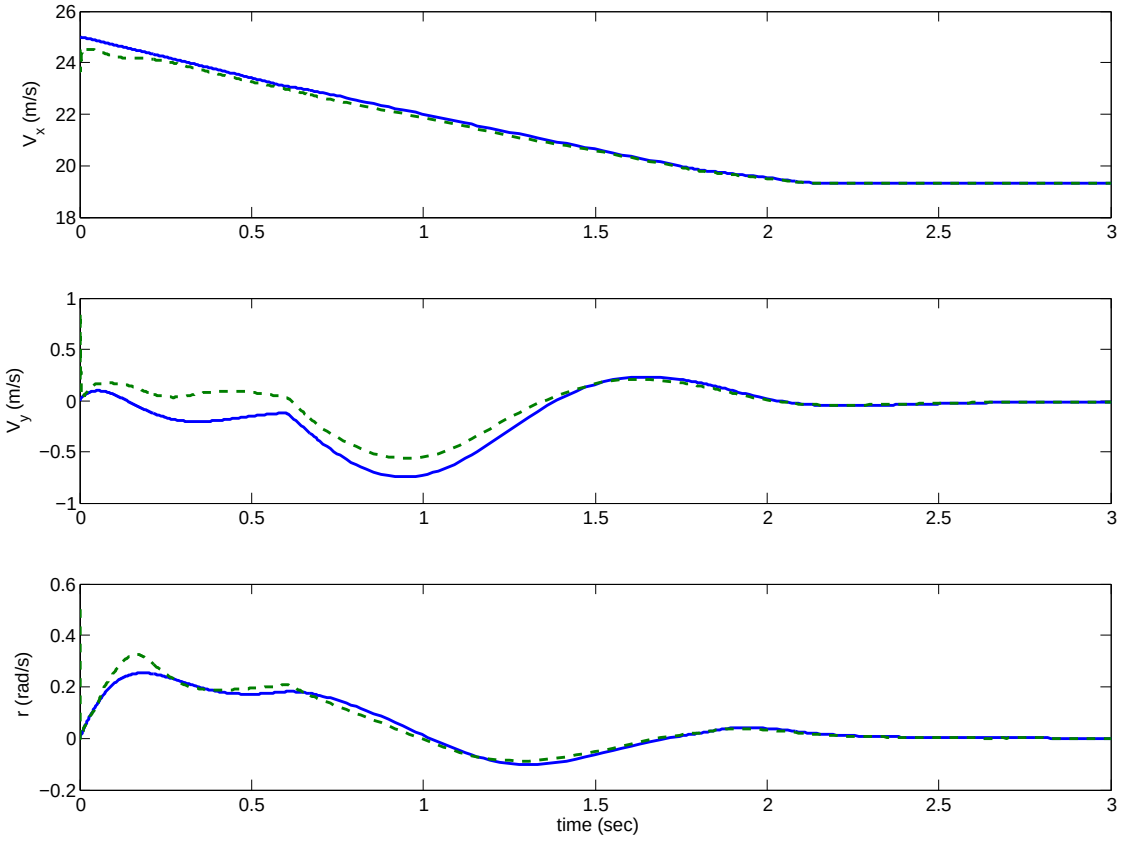

Figure 16: Actual Motion (solid lines) and State Estimates (dashed lines) for v_x, v_y, and r for the Nonlinear Deterministic Approach with $e = 0.5$.

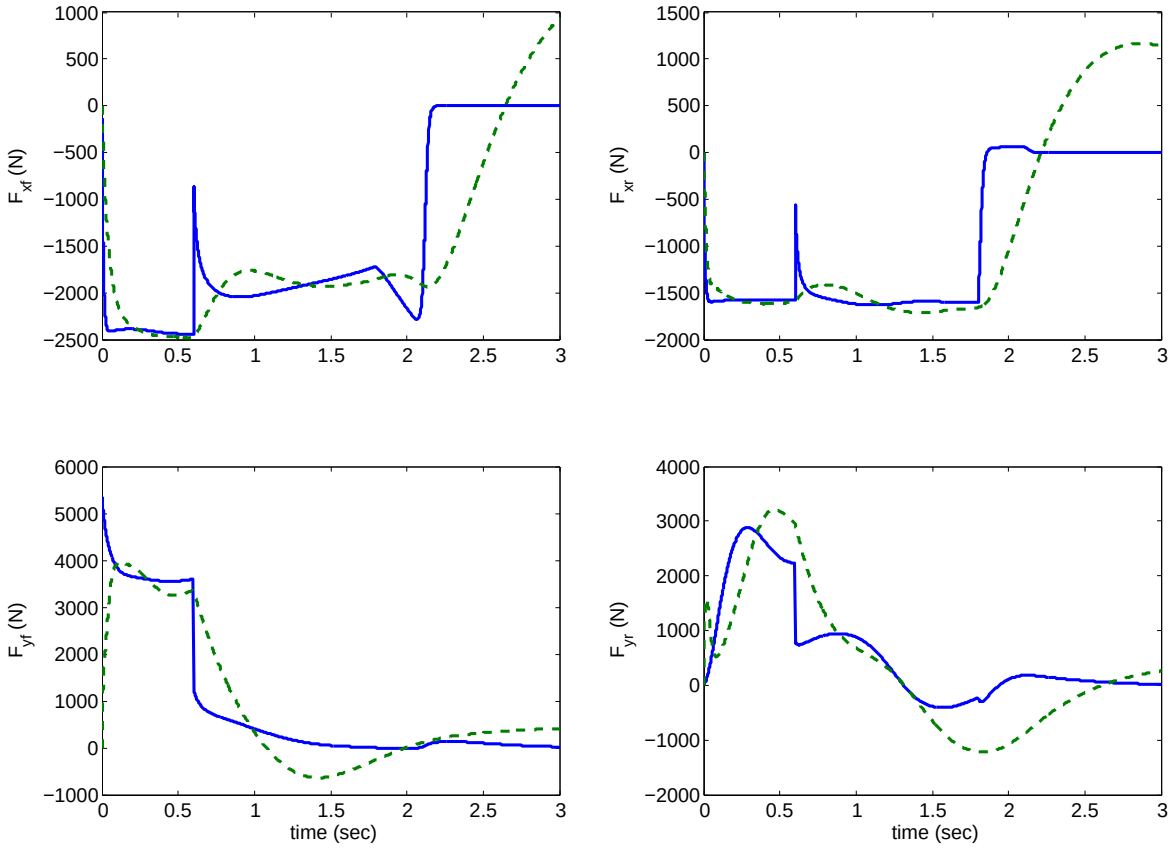

Figure 17: Actual Motion (solid lines) and State Estimates (dashed lines) for F_{xf}, F_{yf}, F_{xr} and F_{yr} for the Linear Stochastic Approach with $e = 0.5$.

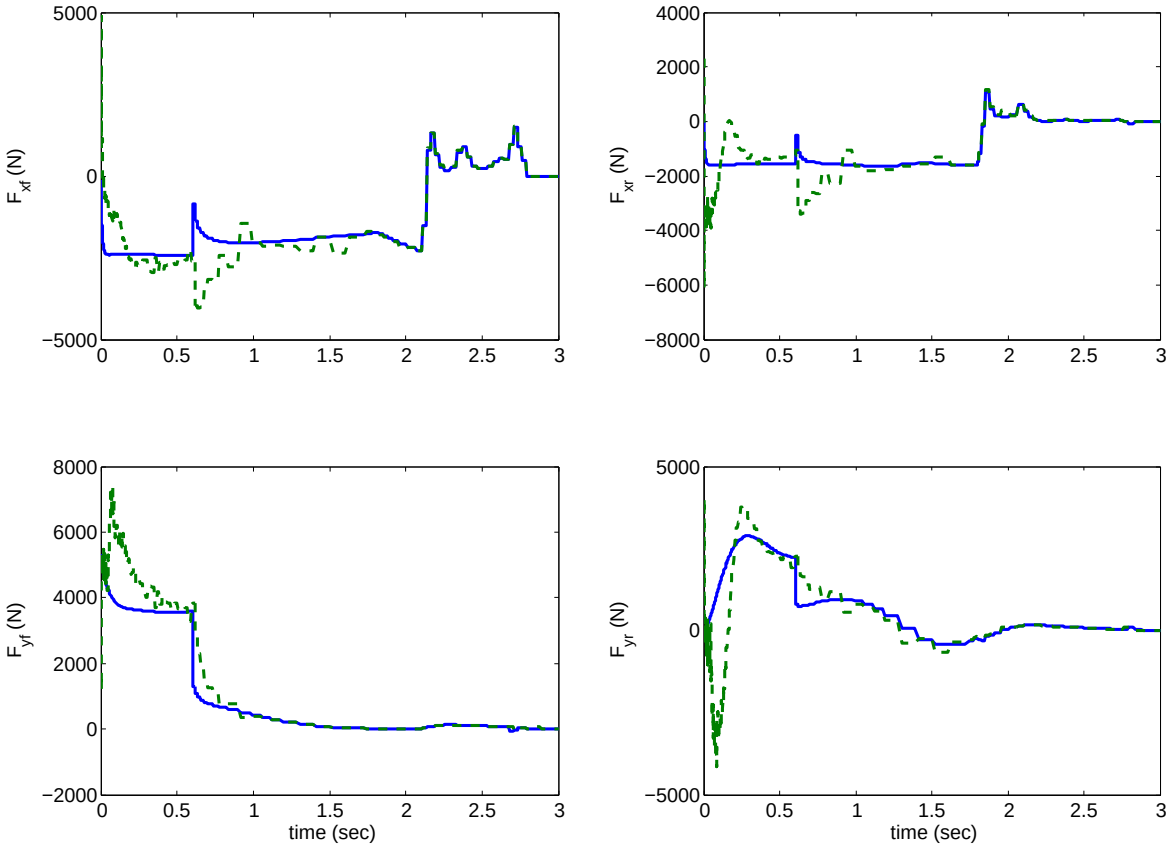

Figure 18: Actual Motion (solid lines) and State Estimates (dashed lines) for F_{xf}, F_{yf}, F_{xr} and F_{yr} for the Nonlinear Deterministic Approach with $e = 0.5$.

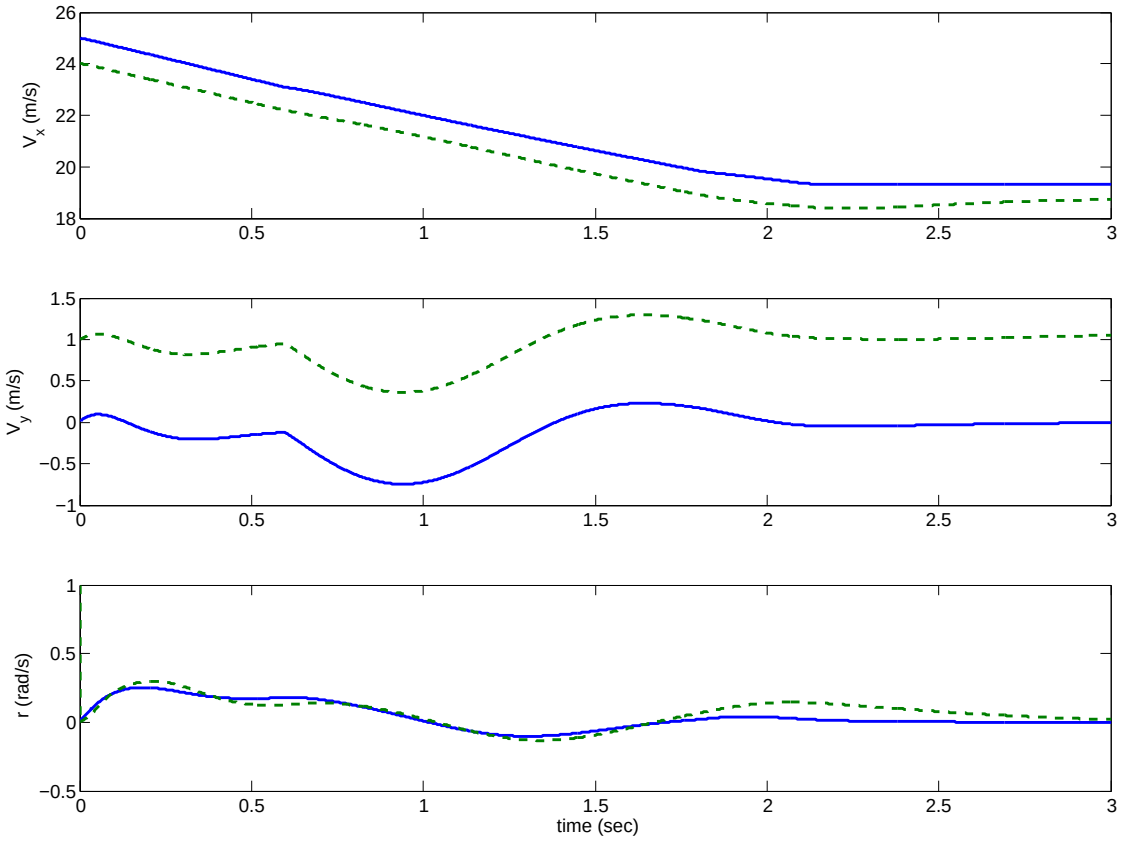

Figure 19: Actual Motion (solid lines) and State Estimates (dashed lines) for v_x, v_y, and r for the Linear Stochastic Approach with $e = 1$.

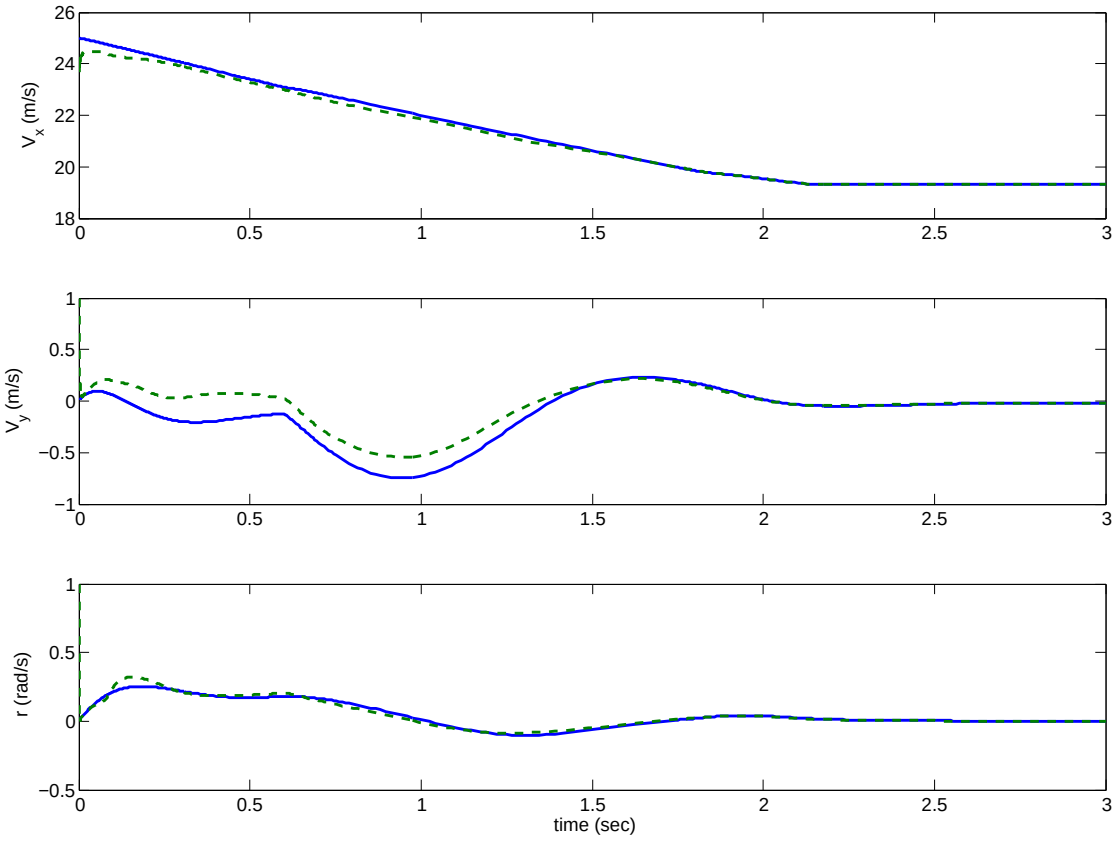

Figure 20: Actual Motion (solid lines) and State Estimates (dashed lines) for v_x, v_y, and r for the Nonlinear Deterministic Approach with $e = 1$.

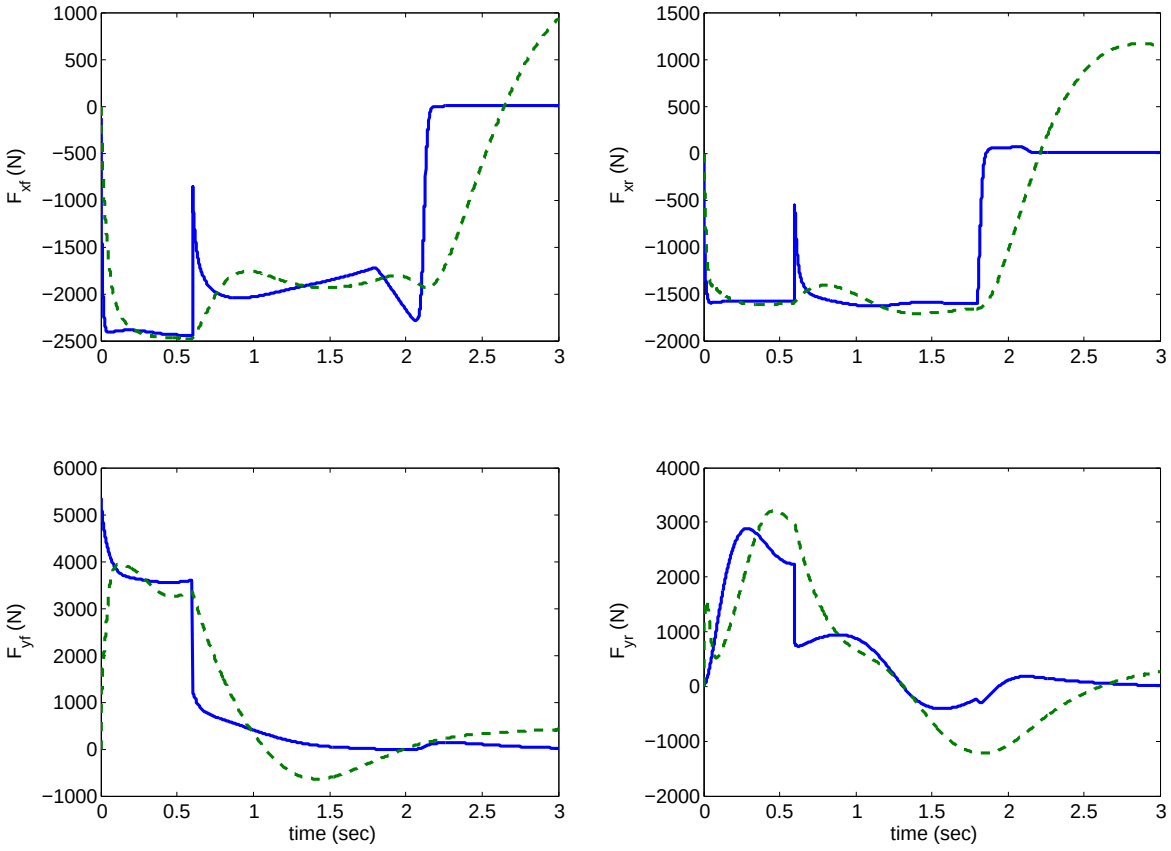

Figure 21: Actual Motion (solid lines) and State Estimates (dashed lines) for F_{xf}, F_{yf}, F_{xr} and F_{yr} for the Linear Stochastic Approach with $e = 1$.

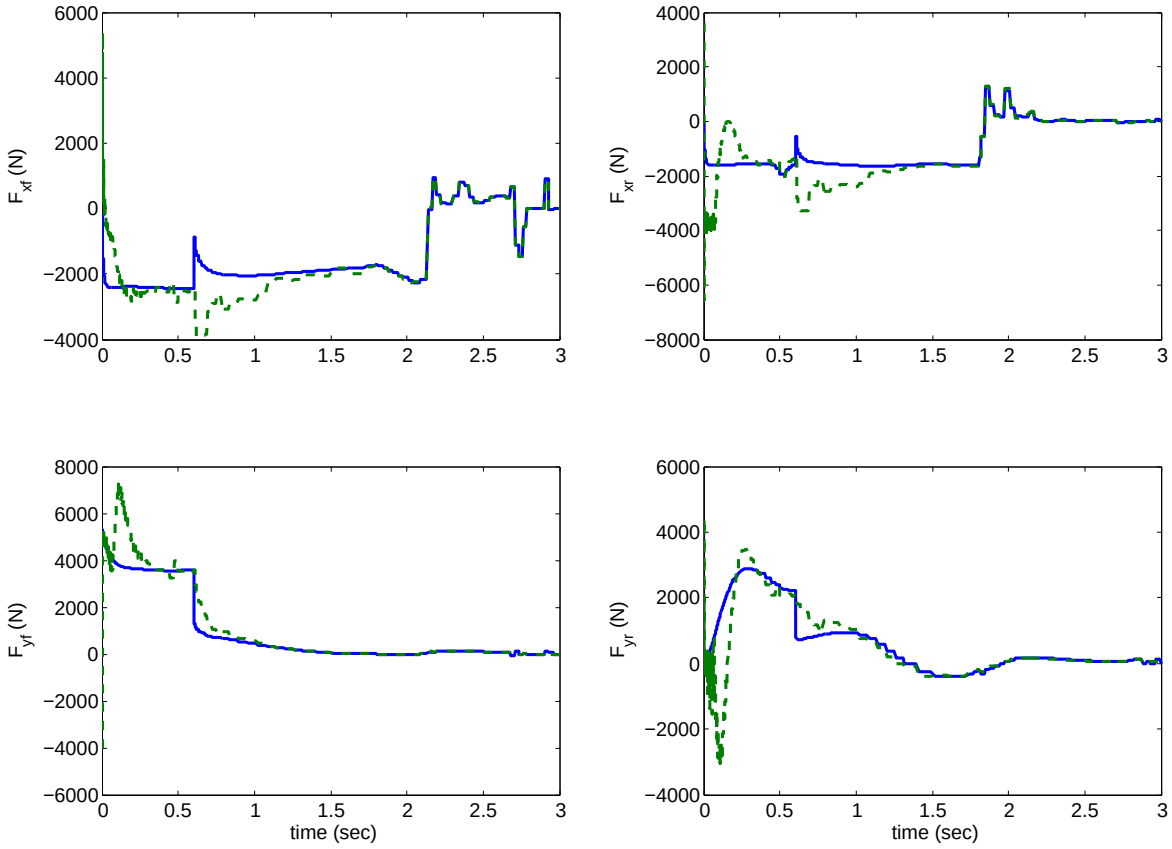

Figure 22: Actual Motion (solid lines) and State Estimates (dashed lines) for F_{xf}, F_{yf}, F_{xr} and F_{yr} for the Nonlinear Deterministic Approach with $e = 1$.

CHAPTER V

CONCLUSION

The main objective of this work was to estimate the longitudinal and lateral velocities of a vehicle using extended Kalman filters. This chapter summarizes the conclusions of this work and discusses possible extensions of the results.

In this work, vehicle dynamics are well-defined, and have been a subject studied by scientists across the years. However, tire force modeling is still a problem, and many researchers are still working on it. In this thesis, three main approaches were implemented: one using a kinematics approach, and the others using a linear stochastic friction model, and a nonlinear deterministic friction model. This work showed the improvement of the results by using the nonlinear deterministic friction model instead of the linear stochastic friction model and the kinematics approach. The kinematics approach uses a really simple estimator, and the results found in Chapter 2 show that if you assume zero slip, you have a lot of error. Moreover, from the results in Chapter 4 for the linear stochastic approach, we can conclude that it is a good approach if you do not have a lot of error between the true model and the estimation model. Finally, from the results in Chapter 4 for the nonlinear deterministic approach, we can conclude that this approach tracks the signal accurately in the cases of this work. Furthermore, we need to remember that in the linear stochastic approach we are obligated to measure brake torque because we do not use a nonlinear deterministic tire-force model. The nonlinear deterministic approach does not need the measurement of the brake torque by replacing the linear stochastic tire-force model with a nonlinear deterministic tire-force model. Therefore, this is the main advantage for the nonlinear deterministic approach in comparison to the linear stochastic approach.

Moreover, the results found in this thesis can be extended to more general situations. First, in 2000, M.C. Best [2] developed a linear deterministic approach to solve this kind of problems. Therefore, a comparison between this approach and the nonlinear deterministic

one can be done.

Furthermore, in [16], Ray implemented a linear stochastic approach in an eight-degree-of-freedom four-wheel vehicle. Consequently, the nonlinear deterministic approach can be generalized to a four-wheel vehicle, and then a comparison can be done between these two approaches.

Finally, the algorithm used in this thesis can be improved trying to use a fixed step algorithm and not the `ode45` function in Matlab that uses a variable step. Another way to improve the algorithm is to use an approximate theory of static analysis to calculate the normal forces. This theory is shown in [9]. In this theory, we suppose no vertical motion using a balance of moments. This theory is a pure approach for a two wheel model. Thanks to this theory, we are not going to calculate the suspension states z_s, $\dot{z}_s$, θ, and $\dot{\theta}$, for this reason, the algorithm is going to be faster.

REFERENCES

[1] Alvarez, L., "Dynamic friction model-based tire-road friction estimation and emergency braking control," *Transactions of the ASME. Journal of Dynamic Systems, Measurement and Control*, vol. 127, pp. 22–32, Mar. 2005.

[2] Best, M., "An extended adaptive kalman filter for real-time state estimation of vehicle handling dynamics," *Vehicle System Dynamics*, vol. 34, pp. 57–75, July 2000.

[3] Bevly, D., "Global positioning system (gps): a low-cost velocity sensor for correcting inertial sensor errors on ground vehicles," *Transactions of the ASME. Journal of Dynamic Systems, Measurement and Control*, vol. 126, pp. 255–264, June 2004.

[4] de Wit, C., "A new nonlinear observer for tire/road distributed contact friction," *42nd IEEE International Conference on Decision and Control*, vol. 3, pp. 2246–2251, 2003.

[5] Detchmendy, D., "The determination of velocity of moving bodies by means of the doppler effect," *Third Congress of the International Federation of Automatic Control*, p. 8, 1966.

[6] Fukada, Y., "Slip-angle estimation for vehicle stability control," *Vehicle System Dynamics*, vol. 32, pp. 375–388, Nov. 1999.

[7] Kehl, S., "Vehicle path-following with a gps-aided inertial navigation system," *Control and Observer Design for Nonlinear Finite and Infinite Dimensional Systems*, pp. 285–300, 2005.

[8] Kiencke, U., "Observation of lateral vehicle dynamics," *Control Engineering Practice*, vol. 5, pp. 1145–1150, Aug. 1997.

[9] Kiencke, U., *Automotive Control Systems*. Springer, first ed., 2000.

[10] Lee, C., "Real-time slip-based estimation of maximum tire-road friction coefficient," *IEEE/ASME Transactions on Mechatronics*, vol. 9, pp. 454–458, June 2004.

[11] Mehra, R., "A comparison of several nonlinear filters for reentry vehicle tracking," *IEEE Transactions on Automatic Control*, vol. 16, pp. 307–319, Aug. 1971.

[12] Muller, S., "Estimation of the maximum tire-road friction coefficient," *Transactions of the ASME. Journal of Dynamic Systems, Measurement and Control*, vol. 125, pp. 607–617, Dec. 2003.

[13] Ramachandra, K., "Estimation of optimum steady-state position, velocity and acceleration from the noisy sampled position data," *Electro-Technology*, vol. 23, pp. 53–59, Sept. 1979.

[14] Ramachandra, K., "Position, velocity and acceleration estimates from the noisy radar measurements," *IEE Proceedings F (Communications, Radar and Signal Processing)*, vol. 131, pp. 167–168, Apr. 1984.

[15] Ray, L. R., "Nonlinear state and tire force estimation for advanced vehicle control," *IEEE Transactions on Control Systems Technology*, vol. 3, pp. 117–124, Mar. 1995.

[16] Ray, L. R., "Nonlinear tire force estimation and road friction identification: simulation and experiments," *Automatica*, vol. 33, pp. 1819–1833, Oct. 1997.

[17] Ryu, J., "Integrating inertial sensors with global positioning system (gps) for vehicle dynamics control," *Transactions of the ASME. Journal of Dynamic Systems, Measurement and Control*, vol. 126, pp. 243–254, June 2004.

[18] Shim, T., "Model-based road friction estimation," *Vehicle System Dynamics*, vol. 41, pp. 249–276, Apr. 2004.

[19] Sivashankar, N., "Yaw rate estimation for vehicle control applications," *Transactions of the ASME. Journal of Dynamic Systems, Measurement and Control*, vol. 120, pp. 267–274, June 1998.

[20] Sri-Jayantha, M., "Determination of nonlinear aerodynamics coefficients using the estimation-before-modeling method," *J. Aircraft*, vol. 25, pp. 796–804, Sept. 1988.

[21] Stephant, J., "Force model comparison on the wheel-ground contact for vehicle dynamics," *IEEE Intelligent Vehicle Symposium. Proceedings*, vol. 2, pp. 589–593, June 2002.

[22] Stephant, J., "Experimental validation of vehicle sideslip angle observers," *IEEE Intelligent Vehicles Symposium*, pp. 150–155, June 2004.

[23] Stephant, J., "Linear observers for vehicle sideslip angle : experimental validation," *IEEE International Symposium on Industrial Electronics*, vol. 1, pp. 341–346, May 2004.

[24] Stephant, J., "Virtual sensor: application to vehicle sideslip angle and transversal forces," *IEEE Transactions on Industrial Electronics*, vol. 51, pp. 278–289, Apr. 2004.

[25] Stephant, J., "Observability matrix and parameter identification: application to vehicle tire cornering stiffness," *Proceedings of IEEE Conference on Decision and Control*, pp. 6734–6739, Dec. 2005.

[26] Ungoren, A., "A study on lateral speed estimation methods," *International Journal of Vehicle Autonomous Systems*, vol. 2, no. 1-2, pp. 126–144, 2004.

[27] Vahidi, A., "Recursive least squares with forgetting for online estimation of vehicle mass and road grade: theory and experiments," *Vehicle System Dynamics*, vol. 43, pp. 31–55, Jan. 2005.

[28] Venhovens, P., "Vehicle dynamics estimation using kalman filters," *Vehicle System Dynamics*, vol. 32, pp. 171–183, Aug. 1999.

[29] Wang, Z., "Estimation of vehicle speed and friction force using moving horizon strategy," *Fifth World Congress on Intelligent Control and Automation*, pp. 1547–1550, June 2004.

[30] Wintergerst, S., "The determination of velocity of moving bodies by means of the doppler effect," *Archiv fur Technisches Messen und Industrielle Messtechnik*, pp. 241–242, Dec. 1958.

[31] Yi, K., "Estimation of tire-road friction using observer based identifiers," *Vehicle System Dynamics*, vol. 31, no. 4, pp. 233–261, 1999.